[12]E. J. Schneid, A. Prakash, and B. L. Cohen, Phys. Rev. 156, 853 (1963).
[13]P. H. Stelson, F. K. McGowan, R. L. Robinson, and W. T. Milner, Phys. Rev. C 2, 2015 (1970).
[14]A. M. Kleinfield, R. Covello-Moro, H. Ogata, G. G. Seaman, G. S. Steadman, and J. De Boer, Nucl. Phys. A154, 499 (1970).
[15]T. K. Kuo, E. U. Baranger, and M. Baranger, Nucl. Phys. 79, 513 (1966); D. M. Clement and E. U. Baranger, *ibid.* A120, 25 (1968); P. L. Ottaviani, M. Savoia, T. Sawicki, and A. Tomasini, Phys. Rev. 153, 1138 (1967). The extensive literature of the application of the quasiparticle–Tamm–Dankoff method can be traced from R. Alzettz, A. Rimini, T. Weber, M. Gmitro, and J. Sawicki, Phys. Rev. 185, 1283 (1969).
[16]P. E. Cavanagh, C. F. Coleman, A. G. Hardacre, G. A. Gard, and J. F. Turner, Nucl. Phys. A141, 97 (1970).
[17]V. K. Thankappan and W. W. True, Phys. Rev. 137, B793 (1965); L. S. Kisslinger and K. Kumar, Phys. Rev. Letters 19, 1239 (1968); A. Goswami and O. Nalcioglu, Phys. Letters 26B, 353 (1968).

PHYSICAL REVIEW C VOLUME 3, NUMBER 6 JUNE 1971

Negative-Parity States in Pb^{208} †

William W. True and Chin W. Ma
Department of Physics, University of California, Davis, California 95616

and

William T. Pinkston
Department of Physics, Vanderbilt University, Nashville, Tennessee 37205

(Received 15 December 1970)

The energies and the detailed structure of the excited states of Pb^{208} with negative parity are well described by a conventional shell-model calculation which uses a "simple" phenomenological residual force. The calculated position of the analog of the ground state of Pb^{208} in Bi^{208} is also in agreement with the experimental results.

I. INTRODUCTION

During the past ten years there have been a great many advances in the field of experimental nuclear physics. These advances have been made possible by better accelerators with both high intensity and good energy resolution. The development of solid-state detectors with their narrow resolution in conjunction with improved accelerators have enabled people to resolve close-lying levels which heretofore has not been possible. This increased resolution is particularly important in the lead region where many excited states appear just a few MeV above the ground state. For example, there are something like 45 observed levels[1,2] (some of which may be multiplets) between 3 and 6 MeV in Pb^{208}.

This increased resolution has enabled one to obtain much better and more precise information on the excited states and ground state of nuclei in the lead region. Most of the recent experimental results on the structure of the energy levels in Pb^{208} are found in Refs. 1–23 and in references contained in these papers.

With this increased experimental information, it is interesting to see if current microscopic nuclear models can explain these results. Of all the regions in the Periodic Table, the lead region has in the past been the most amenable to conventional shell-model calculations where the Pb^{208} nucleus played the role of an "inert core." Thus one would hope to explain the structure of the low-lying states of Pb^{208}, for example, by a shell-model calculation[24,25] (usually called TDA for the Tamm-Dancoff approximation) or by some extension of the shell model[25–28] (one such extension is called RPA for the random-phase approximation).

This paper will describe a shell-model calculation which describes most of the observed structure of the low-lying negative-parity states in Pb^{208} and of the analog of the Pb^{208} ground state which appears as a highly excited state in Bi^{208}. Section II will briefly summarize the pertinent theory which is required to do a TDA calculation for Pb^{208}. The parameters, the single-particle orbitals and the residual nucleon-nucleon force will be discussed in Sec. III where it will be seen that the simple residual force used also consistently explains the structure of other nuclei in the lead region[29,30] and elsewhere.[31,32] The details of the agreement between theory and experiment will be discussed in Secs. IV and V while the wave functions for the lower-lying levels in Pb^{208} are given in Table X.

It should be noted that the excited positive-parity states of Pb^{208} will not be discussed in this paper because we feel that they cannot be adequately described by the truncated basis and the residual force assumed in this paper.

II. THEORY

In this section we will discuss briefly the hole-particle matrix elements necessary for TDA calculations. The most convenient formalism for deriving these matrix elements is that of second quantization. An uncorrelated Pb^{208} ground state is taken as a "vacuum" state or core, and creation and annihilation operators are defined relative to this core. Then the Hamiltonian can be written as

$$H = H_C + H_{Cp} - H_{Ch} + V_{\bar{n}n\bar{n}n} + V_{\bar{p}p\bar{p}p} + V_{\bar{n}n\bar{p}p} + V_{\bar{n}p\bar{n}p} + V' \ . \tag{1}$$

In Eq. (1), H_C is the core energy and consists of the total kinetic energy of all the particles in the core plus their mutual interaction energy. Since all our results will be related to this core energy, we will define this as the zero point in energy.

The term H_{Cp} consists of the kinetic energy of a particle outside the core plus its interaction with the core nucleons. Likewise H_{Ch} represents the kinetic plus potential energy of a hole. The method of obtaining matrix elements of H_{Cp} and H_{Ch} from experiment is discussed in Carter, Pinkston, and True.[24] These matrix elements are diagonal in TDA and RPA calculations. The single-particle energies will be given in the next section.

In our TDA calculation for Pb^{208}, the basis states will consist of neutron hole-neutron particle configurations and of proton hole-proton particle configurations. In Bi^{208}, the basis states will only be neutron hole-proton particle configurations. For Pb^{208}, $V_{\bar{n}n\bar{n}n}$, $V_{\bar{p}p\bar{p}p}$, and $V_{\bar{n}n\bar{p}p}$ will give nonzero matrix elements while only $V_{\bar{n}p\bar{n}p}$ will contribute in Bi^{208} as will be explained below. V' will consist of everything else in the Hamiltonian and will not connect the above one-hole–one-particle configurations to each other. For example, several terms in V' will have three-hole operators and one-particle operator and clearly these terms will not connect the one-hole–one-particle states above. Consequently, we will drop V' from now on.

$V_{\bar{n}n\bar{n}n}$ will act only within and between the neutron-hole–neutron-particle configurations while $V_{\bar{p}p\bar{p}p}$ will act within and between the proton-hole–proton-particle configurations. Since they are both of the same form, we can discuss both of them together as the "like-particle" case. We shall let j represent all the quantum numbers of a particle orbital and $\bar{j}$ represent all the quantum numbers of a hole orbital. Then our basis states will be given by $|\bar{j}_1 j_2 JM\rangle$, where for Pb^{208}, $\bar{j}_1$ and j_2 both refer to neutrons or both refer to protons. In the Bi^{208} case, $\bar{j}_1$ refers to a neutron hole while j_2 refers to a proton particle. The coupling scheme used is to couple l to s to give j (i.e., $\vec{l}+\vec{s}=\vec{j}$) and to couple $\bar{j}_1$ to j_2 to give J (i.e., $\vec{j}_1+\vec{j}_2=\vec{J}$).

For the like-particle case, we have

$$\langle \bar{j}_1 j_2 J | V_{\bar{n}n\bar{n}n} | j_3 j_4 J\rangle = -\sum_K [(1+\delta_{j_1 j_4})(1+\delta_{j_2 j_3})]^{1/2}(2K+1)W(j_1 j_2 j_4 j_3; JK)_a \langle j_2 j_3 K | V | j_4 j_1 K\rangle_a \ , \tag{2}$$

where V is the residual two-body interaction which will be discussed in the next section and the subscript a indicates that antisymmetric states are used in the evaluation of its matrix element. The square-root factor makes Eq. (2) more general than is needed for the TDA calculation because j_1 and j_3 are holes and are never equal to the j_2 and j_4 of the particles. However, in a RPA calculation, this may not be the case and this factor is needed. Note that we could have just as well used $V_{\bar{p}p\bar{p}p}$ above instead of $V_{\bar{n}n\bar{n}n}$.

As implied in Carter, Pinkston, and True[24] and proven in Talman and True,[33] the matrix element in Eq. (2) can be expanded in terms of LS matrix elements and then some of the sums can be made formally. The result can be most conveniently expressed when the residual central force is written in the form

$$V = V(r)(W + MP^r + BP^\sigma + HP^r P^\sigma) \ , \tag{3}$$

where P^r and P^σ are space-exchange and spin exchange operators, respectively. With $A(l_1 l_2 LS|\}j_1 j_2 J)$ representing the LS to jj transformation coefficient, Eq. (2) can be rewritten as

$$\langle \bar{j}_1 j_2 J | V_{\bar{n}n\bar{n}n} | \bar{j}_3 j_4 J\rangle = \sum_{L,S} A(l_1 l_2 LS|\}j_1 j_2 J) A(l_3 l_4 LS|\}j_3 j_4 J) V_{\bar{n}n\bar{n}n}(LS) \ , \tag{4}$$

where $V_{\bar{n}n\bar{n}n}(LS)$ is given by

$$\begin{aligned} V_{\bar{n}n\bar{n}n}(LS) = &-[(W-H)+2(B-M)\delta_{S0}](-1)^{l_2+l_4}\langle l_1 l_2 LS | V(r) | l_3 l_4 LS\rangle \\ &+[(B-M)+2(W-H)\delta_{S0}](-1)^L R^L(l_3 l_2 l_4 l_1)\langle l_3 \| C^L \| l_4\rangle \langle l_2 \| C^L \| l_1\rangle/(2L+1) \ . \end{aligned} \tag{5}$$

In Eq. (5), $R^L(l_3 l_2 l_4 l_1)$ is a Slater integral and $\langle l_3 \| C^L \| l_4 \rangle = [4\pi/(2L+1)]^{1/2} \langle l_3 \| Y_L \| l_4 \rangle$, where $\langle l_3 \| Y_L \| l_4 \rangle$ is the reduced matrix element[34] of $Y_{LM}(\theta, \phi)$.

The $V_{\bar{n}n\bar{p}p}$ term has matrix elements which are given by

$$\langle \bar{j}_1 j_2 J | V_{\bar{n}n\bar{p}p} | \bar{j}_3 j_4 J \rangle = \sum_K (2K+1) W(j_1 j_2 j_4 j_3; JK) \langle j_2 j_3 K | V | j_4 j_1 K \rangle , \tag{6}$$

where j_1 and j_2 refer to neutrons and j_3 and j_4 refer to protons or vice versa. These elements will only appear as off-diagonal matrix elements in the TDA calculation of Pb^{208}. As with the $V_{\bar{n}n\bar{n}n}$ and $V_{\bar{p}p\bar{p}p}$ cases above, we can transform to the LS coupling scheme and do some of the sums. One finds the same equation as is given by Eq. (4) with $V_{\bar{n}n\bar{n}n}$ replaced by $V_{\bar{n}n\bar{p}p}$ and $V_{\bar{n}n\bar{n}n}(LS)$ replaced by $V_{\bar{n}n\bar{p}p}(LS)$, where

$$V_{\bar{n}n\bar{p}p}(LS) = (H + 2M\delta_{S0})(-1)^{l_2+l_4} \langle l_1 l_2 LS | V(r) | l_3 l_4 LS \rangle + (B + 2W\delta_{S0})(-1)^L R^L(l_3 l_2 l_4 l_1) \langle l_3 \| C^L \| l_4 \rangle \langle l_2 \| C^L \| l_1 \rangle / (2L+1) . \tag{7}$$

In Bi^{208}, $V_{\bar{n}n\bar{n}n}$, $V_{\bar{p}p\bar{p}p}$, and $V_{\bar{n}n\bar{p}p}$ do not enter and we only have $V_{\bar{n}p\bar{n}p}$ whose matrix elements are given by

$$\langle \bar{j}_1 j_2 J | V_{\bar{n}p\bar{n}p} | \bar{j}_3 j_4 \rangle = -\sum_K (2K+1) W(j_1 j_2 j_4 j_3; JK) \langle j_2 j_3 K | V | j_4 j_1 K \rangle , \tag{8}$$

where now j_1 and j_2 refer to neutron holes and j_2 and j_4 refer to proton particles. Again we can transform to the LS coupling scheme and the expression for $V_{\bar{n}p\bar{n}p}(LS)$ which replaces $V_{\bar{n}n\bar{n}n}(LS)$ in Eq. (4) is given by

$$V_{\bar{n}p\bar{n}p}(LS) = -(W + 2B\delta_{S0})(-1)^{l_2+l_4} \langle l_1 l_2 LS | V(r) | l_3 l_4 LS \rangle - (M + 2H\delta_{S0})(-1)^L R^L(l_3 l_2 l_4 l_1) \langle l_3 \| C^L \| l_4 \rangle \langle l_2 \| C^L \| l_1 \rangle / (2L+1) . \tag{9}$$

III. SINGLE-PARTICLE ORBITALS AND THE RESIDUAL FORCE

A. Single-Particle Orbitals

Because of practical limitation of computers and available time on the computers, one is forced to several but reasonable approximations in any shell-model calculation.

One of the first considerations is the size of the configuration space which needs to be considered. Before a residual interaction is "turned on," the zeroth order configurations are made up of products of single-particle orbitals where like particles are properly antisymmetrized. In this TDA calculation of Pb^{208}, the zeroth-order configurations consists of one hole in the Pb^{208} core and one particle (same type of particle as the hole) outside the Pb^{208} core. Neutron and proton particles will only be considered in the major shells just above the $N = 126$ and $Z = 82$, respectively. Likewise, we will only consider those neutron and proton holes in the major shells just below $N = 126$ and $Z = 82$, respectively.

One might consider one-hole–one-particle states which are two major shells apart. For harmonic-oscillator orbitals, this would consist of considering orbitals which are separated in energy by $2\hbar\omega$ instead of $1\hbar\omega$ as is the case considered here. One must be very careful in the $2\hbar\omega$ case as two-hole–two-particle configurations from the orbitals separated by $1\hbar\omega$ will lie as low or lower in energy in zeroth order and should be considered also. Secondly, it is not certain what radial dependence should be used for these high-lying orbitals in order to calculate the matrix elements of the residual force. Furthermore, most one-hole–one-particle states formed in this way would have even parity, and only odd-parity levels are considered in the present work.

Under ideal conditions, the single-particle orbitals used should come from some sort of a self-consistent or Hartree-Fock-type calculation. Unfortunately the current Hartree-Fock calculations are not yet good enough to yield a single-particle basis for a shell-model calculation. Consequently, one usually takes the quantum numbers of the single-particle orbitals and their relative separations from the experimental results whenever they are known. It is believed that these single-particle orbitals and their energies are what one would have obtained from a correct self-consistent or Hartree-Fock calculation. The neutron and proton particle and hole orbitals and their relative spacing used in this paper were taken from the paper by Barnes *et al.*[35] and are shown in Fig. 1. Reference 35 also contains additional references concerning the structure and spacings of these single-particle orbitals. The energy "gap" between the holes and particles was taken to be 3.44 MeV for the neutron gap and 4.26 MeV for the proton gap as determined by Carter, Pinkston, and True.[24]

Once the single-particle orbitals are selected, one must decide on the radial form of these orbitals before one can calculate matrix elements. Mathematically it is simpler to use orbitals which have an harmonic-oscillator radial shape since products of two radial orbitals can in a straightforward and relatively simple way be transformed to relative and center-of-mass coordinates.[36,37] Since most conventional residual forces only depend on the relative separation between nucleons, this transformation facilitates the calculation of the radial part of the matrix element.

For the foregoing reasons, the radial dependence of the single-particle orbitals were taken to have an harmonic-oscillator shape with $\nu = 0.1842$ fm^{-2} (see Ref. 29) which corresponds to $\hbar\omega = 7.6$ MeV, where $\psi(r) \sim e^{-\nu r^2/2}$. The tail of the harmonic-oscillator wave functions fall off much more rapidly at large r than, for example, do the wave functions in a Woods-Saxon well. Since most of the contribution to the matrix element comes from the interior region for bound orbitals, one does not expect to have much of an error even though the tails of the wave functions do not behave properly. Indeed, a recent calculation by Kahana, Lee, and Scott (KLS)[38] showed that for the calculated spectra of Pb^{206} and Pb^{210}, the changes caused by replacing the harmonic-oscillator wave functions with Woods-Saxon wave functions were generally small. Clearly this would not be the case for a stripping reaction where the shape and amplitude of the tail are very important. It is also clear for excitations to the higher-lying orbitals which are $2\hbar\omega$ or higher in energy that the radial shape of these single-particle orbitals will be poorly described by an harmonic-oscillator shape. That is, the radial part of the wave function will be more "spread out" than the harmonic-oscillator radial wave functions. In fact, some of these higher-energy single-particle orbitals may lie in the continuum. As a result, the matrix elements of the interaction will be overestimated unless one compensates for this effect.

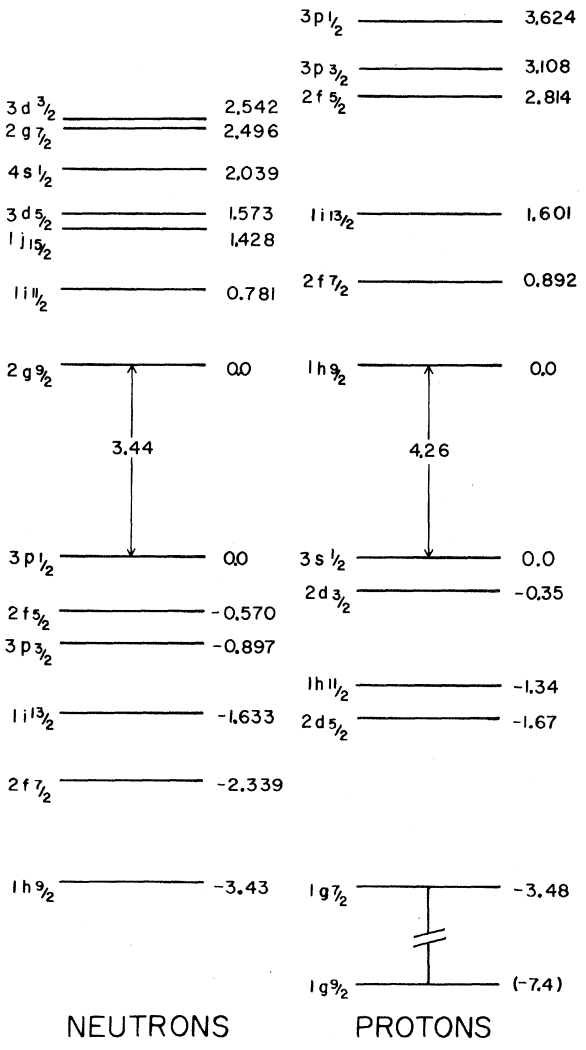

FIG. 1. The experimental single-particle spacings in the lead region from Ref. 35. All energies are in MeV.

Kuo, Blomqvist, and Brown in a calculation[28] on the dipole states in Pb^{208} mentioned that one should use a larger oscillator parameter $\hbar\omega_n$ for neutron orbitals than for proton orbitals. In order to investigate how these different prescriptions of the value of $\hbar\omega$ for the single-particle orbitals will affect our results, we have calculated the levels of Pb^{208} and the analog of the Pb^{208} ground state in Bi^{208} in three different ways. These calculations all use, however, the same residual force as described in Sec. B. In the first calculation a fixed ν of 0.1842 fm^{-2} (or equivalently $\hbar\omega = 7.6$ MeV) was used for all orbitals. In the second calculation the $(\hbar\omega)_{\max}$ as determined by KLS[38] are used. They adjusted the $\hbar\omega$ of each of the orbitals so that maximum overlap between the Woods-Saxon wave function and its main oscillator component was obtained. Finally in the third calculation, the oscillator parameter for the proton orbitals is again set to $\hbar\omega_p = 7.6$ MeV while that of the neutron orbitals is raised arbitrarily to $\hbar\omega_n = 9.4$ MeV which is equal to the $(\hbar\omega)_{\max}$ of the neutron $1j_{15/2}$ orbital. Some of the results are presented in Table I. We observe first that except for a few states, most of the energy levels change by less than 50 keV and many by less than 10 keV as one goes from one $\hbar\omega$ prescription to another. It is interesting to mention here that our choice of $\nu = 0.1842$ fm^{-2} is identical to the average value of $\nu_{\max}$ of KLS[38] taken over all proton and neutron orbitals, i.e., $\langle \nu_{\max} \rangle_{\text{all}} = 0.184$ fm^{-2}, and is also equal to the average value of $\nu_{\max}$ taken over only the neutron-hole

and proton-particle orbitals, i.e., $\langle \nu_{max} \rangle_{\pi p} = 0.184$ fm^{-2}. This probably explains why the first two calculations are so similar in general (see Table I). We see next that the well known 2.61-MeV, 3^- collective state and the 18.0-MeV isobaric analog state (IAS)[39] in Bi^{208} undergo somewhat larger changes. However, the trend is that if one prescription improves the agreement of the calculated 3^- state with the experiment then the agreement of the calculated analog state will be spoiled or vice versa. It is felt that the additional complication of a different ν for each orbital does not give sufficient additional information on the structure of the excited states. Furthermore, the change caused by different prescriptions of $\hbar\omega$ for the single-particle orbitals can be compensated to a large extent by properly adjusting the force parameters in a phenomenological shell-model calculation, consequently all the results quoted in this paper are obtained with a $\nu = 0.1842$ fm^{-2} for all orbitals.

B. Residual Force

Because the Hilbert space used in shell-model calculations is severely truncated, the appropriate residual force for use in such calculations may be considerably different from the free nucleon-nucleon interaction, V_{free}. Included in some way in the residual force must be the effect of virtual transitions outside the model space. It is generally agreed that it makes sense to think of dividing the remainder of Hilbert space into a nearby part and a distant part. Transitions to the distant (very high energy) part, which produce the short-range correlations in the wave function caused by the repulsive core in V_{free}, are accounted for by replacing V_{free} by the Brueckner reaction matrix, G. Once G is determined, the effect of the lower-energy configurations excluded from the model space can be included explicitly by perturbation theory. This is referred to as core polarization.

Numerous authors have calculated G, using procedures which are all formally similar but involving different approximations. We mention here only the pioneering work of Kuo and Brown.[40,41] Great success, especially in light nuclei, has been achieved by this approach; however, it is not clear to us that the method is sufficiently accurate or that the approximation methods are even sufficiently well understood to warrant abandoning the phenomenological approach in heavy nuclei. We feel that this latter approach is justified *a posteriori* by the fact that a relatively simple interaction has been produced which can be used to explain the properties of several nuclei in the lead region. In particular we have been able to obtain a satisfactory simultaneous fit to the 1^- and 3^- collective levels in Pb^{208} and the analog in Bi^{208} of the Pb^{208} ground state. All of these levels are rather sensitive to the input parameters of the calculation.

It was found by True and Ford[29] that the energy level structure of Pb^{206} could be fairly well ex-

TABLE I. The calculated positions of the lowest four eigenstates for the 3^-, 4^-, 5^-, and 6^- levels in Pb^{208} and the positions of the isobaric analog state (IAS) of the ground state of Pb^{208} when the harmonic-oscillator parameters are fixed by three different prescriptions as explained in the text. All energies are in MeV and the residual force described in Sec. III B was used.

I^π	Experimental values	$\hbar\omega_p = \hbar\omega_n = 7.6$ MeV	$(\hbar\omega)_{max}$	$\hbar\omega_p = 7.6$ MeV $\hbar\omega_n = 9.4$ MeV
3^-	2.61	2.49	2.60	1.83
		4.15	4.15	4.17
		4.30	4.17	4.20
		4.71	4.67	4.68
4^-	3.47	3.51	3.52	3.53
		4.07	4.06	4.06
		4.10	4.11	4.12
		4.42	4.43	4.44
5^-	3.19	3.35	3.35	3.17
	3.70	3.68	3.73	3.60
		4.00	3.96	4.00
		4.18	4.18	4.18
6^-	(3.96)	3.98	3.99	3.99
		4.26	4.27	4.27
		4.56	4.55	4.56
		4.58	4.58	4.62
IAS	18.0	17.2	16.6	17.4

plained if a singlet-even central force with a Gaussian shape was used for a residual force. Furthermore, observed $E2$ transitions in Pb^{207} and Pb^{206} indicated the need of including excitations to high-lying orbitals which tend to deform the core and to allow electric multipole transitions to take place which would otherwise be forbidden in the assumed truncated configuration space. By weakly coupling the lower-lying configurations to a high-lying $L=2$ phonon state, it was possible to explain the observed $E2$ transitions and to "mock up" the effect of the phonon admixture on the energy levels by a P_2-type force which we shall call a weak-coupling force and designate it as V_{WC}. With the inclusion of the V_{WC} force, the best fit to the Pb^{206} levels was obtained when the strength of the original singlet-even force (called V_{SE}) was reduced. The "best" residual force was found to be $0.70\ V_{SE}+V_{WC}$ in the calculations of True.[30]

Kuo[42] has applied the Kuo-Brown method[40,41] in the lead region and has found that core-polarization effects do give a P_2-type force correction to the Hamada-Johnston potential which he used as a residual force. The matrix elements in Pb^{206} obtained by Kuo[42] are in good agreement with those of True.[30]

The $0.70\ V_{SE}+V_{WC}$ force will now serve as a guide in our search for a residual interaction to be used in the calculation of Pb^{208} and Bi^{208}. First one generalizes the force to include a triplet-even part. Assuming that it has the same radial dependence as the singlet-even part, we obtain[43]

$$V=\alpha V_0 e^{-\beta r^2}(P^{SE}+\eta P^{TE})+V_{WC} \tag{10}$$

with

$$V_{WC}=\pm\frac{k^2}{C}\sum_{\mu}Y_{2\mu}(\Omega_1)Y^*_{2\mu}(\Omega_2)\ ,$$

where P^{SE} and P^{TE} are the singlet-even and triplet-even projection operators, respectively, $\beta=0.2922$ fm^{-2}, $V_0=-32.5$ MeV. The $\pm$ sign in V_{WC} is given by $(-1)^{n_1+n_2+n_3+n_4+1}$, where the n_i's are the radial quantum numbers of the harmonic-oscillator wave functions which start out with a positive slope at $r=0$. In the case of Pb^{206}, $\alpha=0.70$, $\eta=V_{TE}/V_{SE}=0$ and $k^2/C=1.4$ MeV. Although one does expect a residual force of this type to change somewhat as different nuclei are considered; one still hopes, however, that a force can be found which will explain satisfactorily the experimental data for Pb^{206}, Pb^{208}, and Bi^{208} as well as other nuclei in the lead region. Thus in adjusting the two parameters α and k^2/C for Pb^{208} and Bi^{208}, we shall mainly vary them around their best values as fixed by the calculations of Pb^{206}, namely, 0.70 and 1.4 MeV, respectively.

The triplet-even force does not enter in the Pb^{206} calculations and so no guide as to its strength can be obtained from those calculations. Low-energy scattering data indicate that the triplet-even part of a nucleon-nucleon force is approximately 1.4 to 1.6 times as strong as the singlet-even part of the force. It was found that a ratio of $V_{TE}/V_{SE}\approx 1.6$ gave the best fit in a shell-model calculation[31] of the N^{14} nucleus. The calculation for Pb^{208} and Bi^{208} described in this paper indicates that a slightly larger ratio of $\eta=V_{TE}/V_{SE}$ is needed as will be discussed below.

Experience has shown that the first excited state, a 3^- collective level at 2.61 MeV, in Pb^{208} is very sensitive to the force strength used and to the configuration space adopted. For example, Carter, Pinkston, and True[24] failed to explain the position of this 3^- level because only five hole-particle configurations were considered. In this paper, we have 45 hole-particle configurations which exhaust all the $1\hbar\omega$ excitations that can couple to $J=3^-$. The analog of the ground state of Pb^{208}, a highly excited 0^+ state in Bi^{208} around 18 MeV[39] above the Pb^{208} ground state is also sensitive to the residual force used. Kuo[44] has done a calculation of the energy levels of Bi^{208} using a Hamada-Johnston potential with core-polarization effects included. He found that the calculated position of the analog state was about 4 MeV too low.

It is felt that whatever force one used, it should give about the correct positions for this first 3^- state and the analog state. Indeed, with the information provided by the Pb^{206} calculations, these two states are almost sufficient to fix the force parameters of Eq. (10). We have performed several calculations with different sets of parameters (α,η) while setting $V_{WC}=0$, and some of the results are tabulated in Table II.

TABLE II. The calculated positions of the isobaric analog state (IAS) of the ground state of Pb^{208} and the lowest 3^- level in Pb^{208} as the over-all strength, α, of the residual force, and the triplet-even to singlet-even strength ratio, $\eta=V_{TE}/V_{SE}$, are varied with $V_{WC}=0$ [cf. Eq. (10) in text].

α	$\eta=V_{TE}/V_{SE}$	IAS (MeV)	$E(3^-)$ (MeV)
1.0	1.50	18.2	1.26
0.7	1.50	14.8	2.59
0.7	1.70	16.1	2.35
	1.75	16.5	2.29
	1.80	16.8	2.23
0.75	1.70	16.8	2.12
	1.75	17.2	2.05
	1.80	17.5	1.99
Experimental value		18.0	2.61

It is interesting to observe that by using a force with $\eta = 1.5$, the analog state is calculated to be at 18.2 MeV, which is in good agreement with the observed value. The amplitudes of the various components of this analog state are very close to that predicted for a pure analog state. (See Sec. IV for further discussion of this analog state.) However, this force predicts the first 3^- state to be at 1.26 MeV which is much too low in comparison with the observed position. In fact this force with $\eta = 1.5$ would have to be reduced by a factor of about 0.7 in order to give the correct first 3^- state. However, this large reduction in the force strength would completely destroy the previous good agreement of the analog state which would now be at 14.8 MeV. It is seen that by adjusting the V_{SE} and V_{TE} alone one cannot improve the positions of both the first 3^- state and the analog state at the same time. Table II shows that the best fit is obtained for $\alpha = 0.7$ and $\eta = 1.8$, where the singlet-even part has the same strength as that in the Pb^{206} calculations. If we now add to it the P_2-type force also with the same strength taken from the Pb^{206} calculations, namely $k^2/C = 1.4$ MeV, we obtain the first 3^- state to be at 2.49 MeV and the analog state to be at 17.2 MeV; both are close to the experimental positions. We will use this as our residual force in the present calculations, namely

$$\alpha = 0.7, \quad \eta = V_{TE}/V_{SE} = 1.8, \quad \text{and } \frac{k^2}{C} = 1.4 \text{ MeV}.$$

We would like to mention here that the other energy levels of Pb^{208} are insensitive to small variations in the residual force. The singlet-odd and triplet-odd parts of the residual force are expected to be small and have assumed to be zero since there is no evidence to the contrary. However, it is quite possible that including the V_{TO} and V_{SO} central forces could improve the agreement between theory and experiment. The inclusion of these two odd-state forces would introduce several new parameters into the calculation and this does not appear desirable at this point.

C. TDA or RPA

The lowest 3^- state in Pb^{208} is strongly collective and is observed to have an $E3$ transition strength of about 40 single-particle Weisskopf units.[14-18] In TDA, the collective property for this transition is a result of the hole-particle amplitudes adding coherently in the $E3$ matrix element. Further enhancement is expected from correlations in the ground state (and excited states) from admixtures of n-hole–n-particle configurations. It is believed that most of these correlation effects are taken into consideration by an RPA calculation.

The appropriate residual interaction to use depends on the truncated model space considered. Because RPA calculations allow n hole-n particle admixtures, RPA calculations effectively encompass a larger model space than do the corresponding TDA calculations. Consequently, one does not expect to be able to use the same residual interaction in both a TDA and a RPA calculation. Although TDA and RPA calculations give essentially the same results for most of the levels, the collective levels depend sensitively on the size of the model space and the strength of the force and will differ greatly in position depending on which calculation is done. For example, the TDA calculation described in this paper gave the position of the lowest 3^- level, a collective level, at 2.49 MeV while a RPA calculation with the same residual force gave the position of the energy squared eigenvalue at -3.52 MeV^2. Clearly, this is not the correct residual force to use in a Pb^{208} RPA calculation with the assumed truncated model space. On the other hand, Rowe[45] points out that "higher" RPA treatments tend to increase the energy of low-lying states.

Table II demonstrates that adjustment of the parameters in the potential to make the analog state energy sufficiently high tends to make the energy of the lowest 3^- level too low. Consequently a residual force which would make the lowest 3^- level "correct" in an RPA calculation would give poor results in the TDA calculations of Pb^{206} and Bi^{208}. It should be emphasized that, for the most part, the structure of Pb^{206}, Pb^{208}, and Bi^{208} can be fitted by a single phenomenological interaction and using conventional shell-model procedures which ignore ground-state correlations. Furthermore, it is felt that the structure of the negative-parity excited states of Pb^{208} are adequately described by this residual force even though ground-state correlations have been neglected.

Effective charges[46,47] for electromagnetic transitions are also needed because the space is truncated. These are normally assumed to arise from core polarization, virtual excitations of protons in the core to high-lying orbitals. Since ground-state correlations also are known to enhance electromagnetic transitions, and they are not included in our calculations, the effective charges introduced phenomenologically in this work must contain the effects of both core polarizations and ground-state correlations. In the case of $E1$ transitions, our effective charges must be regarded as compensating for the absence of ground-state correlations. There is no core polarization correction to our $E1$ transitions since the $E1$ strength

to the closed-shell ground state is exhausted by the configurations used.

D. Coulomb Energies

In the Pb^{208} calculation, the proton hole-particle matrix elements will also have a contribution from the Coulomb force. It was observed by Carter, Pinkston, and True[24] that the diagonal matrix elements were quite constant and had a value of about −0.23 MeV while the off-diagonal matrix elements were small and oscillated in sign. Consequently, we shall adopt the prescription[27] of replacing all diagonal Coulomb matrix elements by −0.23 MeV and all off-diagonal Coulomb matrix elements by zero.

IV. ANALOG STATE IN Bi^{208}

The residual force described in Sec. III was used to calculate the structure of ground state and the excited states of Bi^{208} with a neutron-hole–proton-particle basis in the 82 to 126 single-particle orbitals. These results are similar to those obtained by Kim and Rasmussen[48] who used a central potential and a strong tensor component both of which had a Gaussian radial dependence. Our results are also similar to those obtained by Kuo[44] who used an effective force derived from the Hamada-Johnston potential. The details of these calculations for Bi^{208} will be published elsewhere.

However, it is desirable at this point to discuss briefly the position and structure of the analog of the Pb^{208} ground state which is a highly excited 0+ state in Bi^{208}. This analog state is found experimentally to lie approximately at 18 MeV above the Pb^{208} ground state. This value of 18 MeV is obtained by subtracting the neutron-proton mass difference of 0.78 MeV from the Coulomb displacement energy of Pb^{208} which is 18.8 MeV as given by Temmer.[39]

With the residual force described in Sec. III, the analog state is calculated to lie at 17.2 MeV which is close to the observed value of 18 MeV.

The pure analog state is obtained by operating on a closed core for the Pb^{208} ground state with the isospin lowering operator T^-. The squared amplitudes of the neutron-hole–proton-particle states are $2j+1/2T+1$, where j refers to the j of the neutron hole and of the proton particle while $T=22$ is the isotopic spin of the Pb^{208} ground state. The squared amplitudes of the calculated analog state are compared with the $2j+1/2T+1$ factors in Table III.

It is interesting to note that although our residual interaction is charge independent, that we have assumed a pure closed core for the Pb^{208} ground state, and that there is only one $T=22$ state (the others are $T=21$) in our hole-particle configurations, the squared amplitudes for the calculated states are not exactly equal to the $2j+1/2T+1$ values for a pure analog state.

There are two reasons for this lack of perfect agreement. One is that Coulomb forces cause small deviations from isotopic spin purity. The other, more significant reason, is the lack of consistency between the residual interaction and single-particle energies used in the calculation.[49] If the Bi^{208} state in question is the analog of the Pb^{208} ground state, then their binding energies differ only by the Coulomb shift. In a shell-model calculation there must be a perfect cancellation of contributions from the nuclear part of the Hamiltonian, so that the energy eigenvalue of the analog state will come only from the extra Coulomb interaction of the "last" proton in Bi^{208}. This perfect cancellation would occur automatically if the single-particle energies used were calculated theoretically from the assumed residual force by means of a Hartree-Fock calculation. This is because the neutron-hole–proton-particle matrix elements are closely related to the difference between the neutron and proton single-particle energies.[49] Since shell-model calculations are based on single-particle energies obtained from experiment, there is no guarantee of this consistency. The near agreement of the present results with the analog-state energy is a check of the force used against the experimental single-particle energies. The reproduction of the analog-state wave function expected from isotopic spin purity is indirect evidence for "almost" charge-independent nuclear forces.

V. DISCUSSION OF RESULTS FOR Pb^{208}

The residual force described in Sec. III was used in a TDA calculation to obtain the detailed structure of the excited states of Pb^{208}. The calculated energies and eigenfunctions for the low-lying negative-parity states are given in Table X. In this section, we will describe in some detail the agreement between the calculated results and the experimental ones. The four lowest excited states have been studied in more detail, since it is more difficult to resolve the individual levels for higher excitation energies. Consequently we will be able to discuss the first four excited states one at a time and only compare the higher-lying states in groups which is also how the experimental results are given in general.

A. 2.608 MeV, 3^- Level

This well-known collective state in Pb^{208} was calculated to be at 2.49 MeV which is in good agree-

TABLE III. Comparison between the squared amplitudes of the calculated 17.2-MeV 0^+ state in Bi^{208} and those of a pure analog state. T is the isospin of the Pb^{208} ground state.

$\lvert\bar{j}_n j_p\rangle$	$\lvert\bar{h}_{9/2}h_{9/2}\rangle$	$\lvert\bar{f}_{7/2}f_{7/2}\rangle$	$\lvert\bar{i}_{13/2}\,i_{13/2}\rangle$	$\lvert\bar{f}_{5/2}f_{5/2}\rangle$	$\lvert\bar{p}_{3/2}p_{3/2}\rangle$	$\lvert\bar{p}_{1/2}p_{1/2}\rangle$
This calculation	0.24	0.19	0.26	0.15	0.12	0.05
$\frac{2j+1}{2T}$	0.23	0.18	0.32	0.14	0.09	0.05

ment with the observed value of 2.61 MeV. The collectivity of this state is demonstrated by the fact that it has a large $E3$ transition strength (about 40 Weisskopf single-particle units[14-18]) for decay to the ground state of Pb^{208}. The (p, p') experiments of Zaidi *et al.*[3] to this 3^- state show resonances at the analog states in Bi^{209} of all the single-particle neutron states in Pb^{209}. These observations imply that the 3^- state has many neutron hole-particle components which is also consistent with it being a collective state. Indeed our calculated eigenfunction (see Table X) for this state is a multiconfiguration eigenfunction with no one or two components dominating it.

Bjerregaard *et al.*[11, 12] and McClatchie, Glashausser, and Hendrie[13] have studied the proton hole-particle structure of the lowest four excited states in Pb^{208} by (t, α) and (d, He^3) reactions, respectively, with Bi^{209} as a target. These experiments enable one to deduce the relative spectroscopic factors of the larger $\lvert\bar{l}j, h_{9/2}\rangle_p$ components. The relative proton hole-particle spectroscopic factors are defined as

$$S_{lj}(p) = (2J+1)\chi_{lj}^2(p)/(2I+1)\,, \qquad (11)$$

where J is the spin of the Pb^{208} excited state, $I = \frac{9}{2}$ is the spin of the Bi^{209} ground state, and $\chi_{lj}(p)$ is the amplitude for the $\lvert\bar{l}j, h_{9/2}\rangle_p$ proton hole-particle component in the eigenfunction. The calculated S_{lj}'s given by Eq. (11) are compared with the experimentally measured S_{lj}'s in Table IV. Bjerregaard *et al.*[12] have put upper limits on many of the spectroscopic factors. This only means that if the spectroscopic factors were larger than the given upper limit, then they would have been observed. On the other hand, they could be smaller and our calculated values seem to indicate this. In general, the measured and experimental spectroscopic factors are in agreement.

We would also like to point out that the calculated results given in Table IV are similar to the unpublished results of Kuo and of Gillet which are quoted by Bjerregaard *et al.*[12]

We have used our wave function to calculate the quadrupole moment of this 3^- state adopting an effective charge of $0.5e$ as described in Sec. V H. The calculated result is $Q_{\text{calc}} = -0.061$ b which is about 20 times smaller than the experimental value of $Q_{\text{exp}} = -1.3 \pm 0.6$ b as measured by Barnett and Phillips.[17] It is not clear to us why the discrepancy is so large.

B. 3.192 MeV, 5^- Level

The lowest 5^- level is calculated to be at 3.35 MeV which is in agreement with the observed energy of 3.19 MeV. The calculated $\lvert\bar{s}_{1/2}, h_{9/2}\rangle_p$ spec-

TABLE IV. The relative spectroscopic factors for the $\lvert\bar{l}j, h_{9/2}\rangle_p$ proton hole-particle states in Pb^{208}. The experimental results were taken from Ref. 12 and Ref. 13.

E (MeV)	I^π		$\lvert\bar{s}_{1/2}, h_{9/2}\rangle_p$	$\lvert\bar{d}_{3/2}, h_{9/2}\rangle_p$	$\lvert\bar{d}_{5/2}, h_{9/2}\rangle_p$	$\lvert\bar{g}_{7/2}, h_{9/2}\rangle_p$
2.608	3^-	exp (Ref. 13)		0.18		
		exp (Ref. 12)	0	≤0.10	≤0.07	≤0.28
		This calculation	0	0.11	0.005	0.023
3.192	5^-	exp (Ref. 13)	0.08			
		exp (Ref. 12)	0.06	<0.09	<0.06	<0.28
		This calculation	0.044	0.023	0.003	0.002
3.469	4^-	exp (Ref. 13)				
		exp (Ref. 12)	≤0.004	≤0.007	≤0.005	≤0.02
		This calculation	0.000 02	0.0001	0.000 02	0.000 008
3.702	5^-	exp (Ref. 13)	0.42			
		exp (Ref. 12)	0.31	<0.52	<0.36	<1.7
		This calculation	0.30	0.038	0.002	0.002

troscopic factor of 0.044 for this level is in agreement with the two measured values of 0.08 and 0.06 which are given in Table IV.

Bardwich and Tickle (BT)[9] have studied this level by the $Pb^{207}(d, p)Pb^{208}$ reaction which should populate the $|\bar{p}_{1/2}, lj\rangle_n$ components of this state. They found that this state is dominated by the $|\bar{p}_{1/2}, g_{9/2}\rangle_n$ component – a result also favored by Sastry[21] in his study of the β decay of Tl^{208}. The calculated result is in agreement with these experimental results and has a value of 0.92 for the amplitude of the $|\bar{p}_{1/2}, g_{9/2}\rangle_n$ configuration (see Table X).

BT have also extracted relative neutron hole-particle spectroscopic factors which are defined by

$$(2J+1)S_{lj}(n) = (2J+1)\chi_{lj}^2(n) , \qquad (12)$$

where J is the spin of the Pb^{208} level and $\chi_{lj}(n)$ is the amplitude of the $|\bar{p}_{1/2}, lj\rangle_n$ neutron hole-particle component. For the $|\bar{p}_{1/2}, g_{9/2}\rangle_n$ component of the 3.19-MeV level, the calculated value of 9.4 is in excellent agreement with the experimental value of 9.5. The relative spectroscopic factors for the other $|\bar{p}_{1/2}, lj\rangle_n$ components of this level and for other levels will be discussed in Sec. V E.

C. 3.469-MeV, 4⁻ Level

Our lowest calculated 4^- level lies at 3.51 MeV and the eigenfunction is given by

$$\psi_{\text{calc}}(3.51, 4^-) = 0.94|\bar{p}_{1/2}, g_{9/2}\rangle_n - 0.23|\bar{p}_{3/2}, g_{9/2}\rangle_n - 0.25|\bar{f}_{5/2}, g_{9/2}\rangle_n ,$$

where the other components which are less than 1% have been neglected. This level has been studied experimentally by Bondorf, von Brentano, and Richard[5] by a (p, p') reaction and they found a structure for this level of

$$\psi_{\text{exp}}(3.47, 4^-) = (0.96 \pm 0.02)|\bar{p}_{1/2}, g_{9/2}\rangle_n - (0.26 \pm 0.03)|\bar{p}_{3/2}, g_{9/2}\rangle_n + (0.07 \mp 0.16)|\bar{f}_{5/2}, g_{9/2}\rangle_n .$$

The first two amplitudes agree very well. The $|\bar{f}_{5/2}, g_{9/2}\rangle_n$ amplitudes do not agree. On the other hand, this amplitude is not too well determined experimentally.

BT[9] have measured the relative spectroscopic factor as defined by Eq. (12) to be 8.7 for the $|\bar{p}_{1/2}, g_{9/2}\rangle_n$ component and the calculated value is 8.0 which is in good agreement.

This level does not resonate at the other analog resonances in the (p, p') experiments besides those three mentioned above and is absent in the $Bi^{209}(t, \alpha)Pb^{208}$ and $Bi^{209}(d, He^3)Pb^{208}$ experiments which indicate that the amplitudes of all the other neutron and proton hole-particle configurations are very small. Indeed this is the case for our calculated eigenfunction and the squared amplitudes of all the hole-particle components except those mentioned above are less than 1%.

D. 3.702-MeV, 5⁻ Level

Our second 5^- level is calculated to be at 3.68 MeV and

$$\psi_{\text{calc}}(3.68, 5^-) = 0.29|\bar{p}_{1/2}, g_{9/2}\rangle_n + 0.18|\bar{p}_{3/2}, g_{9/2}\rangle_n - 0.57|\bar{f}_{5/2}, g_{9/2}\rangle_n + 0.36|\bar{p}_{1/2}, i_{11/2}\rangle_n + 0.19|\bar{f}_{5/2}\, i_{11/2}\rangle_n + 0.11|\bar{i}_{13/2}\, j_{15/2}\rangle_n ,$$

where only the large neutron hole-particle components are given (see Table X for more detail). Richard *et al.*[7] have experimentally determined the neutron hole-particle structure of this level to be

$$\psi_{\text{exp}}(3.70, 5^-) = (0.41 \pm 0.02)|\bar{p}_{1/2}, g_{9/2}\rangle_n + (0.10 \mp 0.18)|\bar{p}_{3/2}, g_{9/2}\rangle_n - (0.76 \pm 0.12)|\bar{f}_{5/2}, g_{9/2}\rangle_n .$$

Here the agreement of the amplitudes is not as impressive as before but the agreement is still reasonably good. Richard *et al.*[7] however point out that the experimental amplitudes given above could possibly be questioned since their analysis was made by assuming a pure compound cross section which ignored a measurable direct component.

The proton hole-particle relative spectroscopic factors defined by Eq. (11) of this level are compared to the experimental results of Bjerregaard *et al.*[11] and McClatchie, Glashausser, and Hendrie[13] in Table IV. Again good agreement between the calculations and the experimental results are obtained. Also the calculated configurations are in agreement with the β-decay studies of Tl^{208} by Shastry.[21]

Mukherjee and Cohen[1] and BT[9] observed the broadening of a line in this region in their Pb^{207}-$(d, p)Pb^{208}$ experiments and concluded that there was a doublet of levels at 3.73 and 3.76 MeV. BT concluded that these states were dominated by the $|\bar{p}_{1/2}, g_{9/2}\rangle_n$ component although they failed to resolve the two levels. The (p, p'), (t, α), and (d, He^3) experiments mentioned above observed only one level, a 5^- level at 3.702 MeV, in this energy region. Our next higher calculated level lies at 3.98 MeV and is dominated by a very pure $|\bar{f}_{5/2}, g_{9/2}\rangle_n$ hole-particle configuration. Furthermore if one calculates the spectroscopic factor of the 5^- level at 3.70 MeV using the experimental determined[7]

value of 0.41 as the amplitude of its $|\bar{p}_{1/2}, g_{9/2}\rangle_n$ component; one obtains, according to Eq. (12), $(2J+1)S(n) = 1.85$ which is in excellent agreement with the value of 1.9 as measured by BT for the conjectured doublet. Thus it is quite possible that there is only one 5^- level in this energy region.

E. Relative Spectroscopic Factors and Centers of Gravity

Above about 3.8 MeV the excited levels in Pb^{208} became so dense that it is difficult to resolve them and to experimentally study them in detail as has been done for the lowest four levels. For the higher-energy regions, the experimental results are given in the form of spectroscopic information for groups of levels, centroid energies for various hole-particle multiplets, and total strength for various hole-particle multiplets. We will now compare our calculated results for the negative-parity states in this manner.

As mentioned above, the relative spectroscopic factors defined by Eq. (12) for the neutron hole-particle configurations, $|\bar{p}_{1/2}, lj\rangle_n$, have been measured by BT[9] by the $Pb^{207}(d, p)Pb^{208}$ reaction. The relative spectroscopic factors defined by Eq. (11) for the proton hole-particle configurations, $|\bar{l}\bar{j}, h_{9/2}\rangle_p$, have been measured by Bjerregaard *et al.*[12] by the $Bi^{209}(t, \alpha)Pb^{208}$ reaction and by McClatchie, Glashausser, and Hendrie[13] by the Bi^{209}-$(d, He^3)Pb^{208}$ reaction. These measured spectroscopic factors provide a direct test of our calculated wave functions.

Our first comparison will be for the total strength of a given hole-particle multiplet. For the (d, p) reaction the total strength of a given neutron hole-particle multiplet is defined by

$$\sum(2J+1)S_{lj}(n) = \sum_J(2J+1)\,, \tag{13}$$

where $S_{lj}(n)$ is defined in Eq. (12) and the J's are the possible spins which can be obtained by coupling a $p_{1/2}$ neutron hole to a lj neutron particle. The summation at the left-hand side is to be taken over all states which share the $|\bar{p}_{1/2}, lj\rangle_n$ hole-particle strength. For the (t, α) and (d, He^3) reactions, the total strength of a given proton hole-particle multiplet is defined by

$$\sum S_{lj}(p) = 2j+1\,, \tag{14}$$

where $S_{lj}(p)$ is defined in Eq. (11), j is the spin of the transferred proton hole, and the sum is over all the levels which share the $|\bar{l}\bar{j}, h_{9/2}\rangle_p$ hole-particle strength.

The total theoretical strengths, the experimentally measured strengths, and the calculated strengths for neutron and proton hole-particle multiplets are compared in Tables V and VI, respectively. In summing up the calculated total strength we have omitted the contributions from those levels in which the amplitude of the hole-particle component under consideration is smaller than 0.06. In Table V, the experimental measurements only considered excited states below 6.1-MeV excitation and consequently the calculated strengths also included only those calculated levels below 6.1 MeV. It can be seen from Table V that the experimental and calculated strengths agree very well. Both the $|\bar{p}_{1/2}, g_{7/2}\rangle_n$ and $|\bar{p}_{1/2}, d_{3/2}\rangle_n$ experimental and calculated strengths are somewhat below the sum-rule value. This is mostly due to the energy cutoff at 6.1 MeV. Indeed, if all the levels below 7.1 MeV were included, the calculated total strength will increase to 7.51 and 15.5 for the $|\bar{p}_{1/2}, d_{3/2}\rangle_n$ and $|\bar{p}_{1/2}, g_{7/2}\rangle_n$ multiplets, respectively. The additional missing strength is expected to be shared by levels lying at even higher energy.

In Table VI we see that the experimental and calculated proton total strengths of the $|\bar{s}_{1/2}, h_{9/2}\rangle_p$ and $|\bar{d}_{3/2}, h_{9/2}\rangle_p$ multiplets agree very well. They are slightly below the values predicted by the sum rule which is to be expected since only the states below 5.7 MeV were considered in determining both the experimental and calculated strengths. The agreement for the total strength of the $|\bar{d}_{5/2}, h_{9/2}\rangle_p$ multiplet is not as good as the above two; its calculated value is less than the experimental one even

TABLE V. Sum rule of the total strength for the neutron hole-particle multiplets in Pb^{208}. The experimental results were taken from Ref. 9.

Multiplet	$\sum(2J+1)S$ Sum rule	$\sum(2J+1)S_{\text{exp}}$	$\sum(2J+1)S_{\text{calc}}$
$\|\bar{p}_{1/2}, g_{9/2}\rangle_n$	20	20.7	19.7
$\|\bar{p}_{1/2}, i_{11/2}\rangle_n$	24	23.2	23.8
$\|\bar{p}_{1/2}, d_{5/2}\rangle_n$	12	10.4	11.5
$\|\bar{p}_{1/2}, s_{1/2}\rangle_n$	4	3.6	3.4
$\|\bar{p}_{1/2}, g_{7/2}\rangle_n$	16	11.7	14.2
$\|\bar{p}_{1/2}, d_{3/2}\rangle_n$	8	4.3	5.8

TABLE VI. Sum rule of the total strength for the proton hole-particle multiplets in Pb^{208}. The experimental results were taken from Ref. 13.

Multiplet	$\sum S$ Sum rule	$\sum S_{\text{exp}}$	$\sum S_{\text{calc}}$
$\|\bar{s}_{1/2}, h_{9/2}\rangle_p$	2	1.96	1.97
$\|\bar{d}_{3/2}, h_{9/2}\rangle_p$	4	3.83	3.95
$\|\bar{d}_{5/2}, h_{9/2}\rangle_p$	6	5.61	4.77

though in this case all calculated levels up to 5.9 MeV are included in the summation. We also notice in Tables V and VI that in general the agreement of the calculated strengths with the experiment is better for the low-lying multiplets than for the high-lying multiplets.

It is rewarding that the calculated and experimental strengths of the neutron and proton multiplets are in the same energy region. If the experimental strengths were considerably lower than the calculated strengths, one would have been forced to conclude that the fractionation of the strength had occurred with some of the strength appearing at higher energies due to mixing of more complicated configurations with the one-hole–one-particle configurations. Then our truncated space of one-hole–one-particle configurations would have been inadequate to explain the experimental observations.

Our next comparison between the calculated results and the experimental results will be to look at the spectroscopic factors in more detail. Since it is essentially impossible to identify level by level the calculated and the observed levels, the comparison will be presented by graphs. The relative spectroscopic factors defined by Eq. (12) for the neutron hole-particle components are compared with the experimental results of BT[9] in Fig. 2. Similarly the relative proton hole-particle spectroscopic factors defined by Eq. (11) are compared with the experimental results of McClatchie, Glashausser, and Hendrie[13] in Fig. 3.

Figures 2 and 3 indicated clearly that the agreement between the experimental and calculated results are generally good. The general features like the occurrence of clusters, their widths, and their locations are well reproduced by the calculations.

Another comparison which can be made is the center of gravity of the hole-particle multiplets. The center of gravity of the proton multiplets is

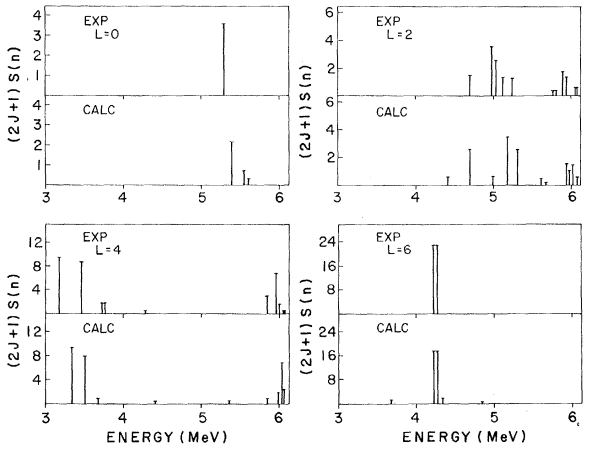

FIG. 2. Relative spectroscopic factors for the $|p_{1/2}, lj\rangle_n$ neutron hole-particle configurations. The experimental results were taken from Ref. 9. The double lines indicate a doublet.

defined by

$$\bar{E}_{lj}(p) = \sum_J \frac{S_{lj}(p) E_J}{2j+1} \tag{15}$$

and the center of gravity of the neutron multiplets is defined by

$$\bar{E}_{lj}(n) = \sum_J (2J+1) S_{lj}(n) E_J / \sum_J (2J+1) \ . \tag{16}$$

In Eqs. (15) and (16), the sum over J is over all levels which contain the given multiplet.

The calculated and experimental centers of gravity for the $|\bar{p}_{1/2}, lj\rangle_n$ hole-particle multiplets and the $|\bar{l}j, h_{9/2}\rangle_p$ hole-particle multiplets are compared in Tables VII and VIII, respectively. In Table VIII, one notes that the calculated centers of gravity of the proton multiplets are about 150 keV larger than the experimental ones and that both are lower than the zeroth-order energies. In Table VII, one sees that the calculated and experimental neutron centers of gravity are in better agreement with each other.

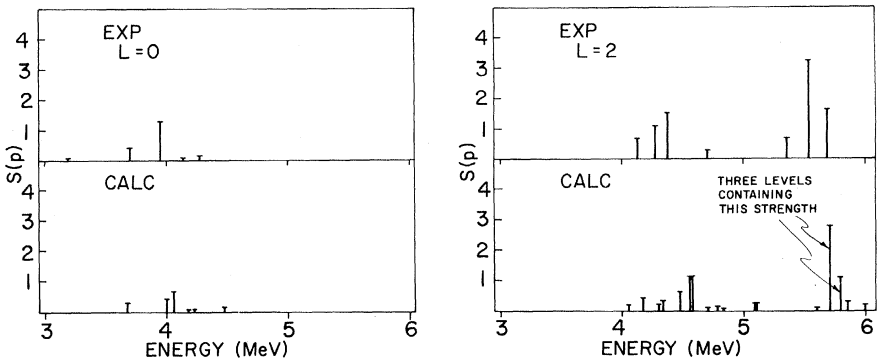

FIG. 3. Relative spectroscopic factors for the $|\bar{l}j, h_{9/2}\rangle_p$ proton hole-particle configurations. The experimental results were taken from Ref. 13. The double lines indicate doublets.

TABLE VII. Centroid energies of the neutron hole-particle multiplets in Pb^{208}. E_0 is the zeroth-order energy. The experimental results were taken from Ref. 9.

Multiplet	E_0 (MeV)	$\bar{E}_{exp}$ (MeV)	$\bar{E}_{calc}$ (MeV)	$\bar{E}_{calc}-\bar{E}_{exp}$ (MeV)
$\vert\bar{p}_{1/2}, g_{9/2}\rangle_n$	3.44	3.39	3.50	0.11
$\vert\bar{p}_{1/2}, i_{11/2}\rangle_n$	4.21	4.25	4.26	0.01
$\vert\bar{p}_{1/2}, d_{5/2}\rangle_n$	5.00	5.00	5.07	0.07
$\vert\bar{p}_{1/2}, s_{1/2}\rangle_n$	5.47	5.28	5.46	0.18
$\vert\bar{p}_{1/2}, g_{7/2}\rangle_n$	5.91	5.94	5.90	−0.04
$\vert\bar{p}_{1/2}, d_{3/2}\rangle_n$	5.96	5.92	5.90	−0.02

TABLE VIII. Centroid energies of the proton hole-particle multiplets in Pb^{208}. E_0 is the zeroth-order energy. The experimental results were taken from Ref. 13.

Multiplet	E_0 (MeV)	$\bar{E}_{exp}$ (MeV)	$\bar{E}_{calc}$ (MeV)	$\bar{E}_{calc}-\bar{E}_{exp}$ (MeV)
$\vert\bar{s}_{1/2}, h_{9/2}\rangle_p$	4.23	3.90	4.09	0.19
$\vert\bar{d}_{3/2}, h_{9/2}\rangle_p$	4.58	4.25	4.42	0.17
$\vert\bar{d}_{5/2}, h_{9/2}\rangle_p$	5.90	5.55	5.66	0.11

F. Total Inelastic Proton Partial Width

Richard *et al.*[7] have measured the proton partial widths Γ_p for exciting the $\vert\overline{lj}, g_{9/2}\rangle_n$ hole-particle configurations in Pb^{208} from a $Pb^{208}(p, p')Pb^{208*}$ analog resonance reaction. The proton partial width is given by

$$\Gamma_p = \sum_j \frac{(2J+1)\Gamma_{lj}^{SP}\chi_{lj,l'j'}^{\,2}}{2j'+1}\,, \tag{17}$$

where J is the spin of the final state in Pb^{208}, $l'j'$ are the quantum numbers of the neutron in the parent analog state $-g_{9/2}$ in this case, lj are the quantum numbers of the neutron hole state, $\chi_{\overline{lj},l'j'}$ is the amplitude for the $\vert\overline{lj}, l'j'\rangle_n$ component, and Γ_{lj}^{SP} is the single-particle width. In this sum over j, we will neglect the $i_{13/2}$ and $h_{9/2}$ neutron hole states because they are only weakly populated due to the high angular momentum barrier. Note that the partial widths depend on the $\vert\bar{p}_{1/2}, g_{9/2}\rangle_n$, $\vert\bar{f}_{5/2}, g_{9/2}\rangle_n$, $\vert\bar{p}_{3/2}, g_{9/2}\rangle_n$, and $\vert\bar{f}_{7/2}, g_{9/2}\rangle_n$ amplitudes and this provides a further test of these neutron hole-particle configurations in our calculated wave functions. This is in contrast to the spectroscopic factors obtained from the $Pb^{207}(d, p)Pb^{208}$ experiments which only tests the $\vert\bar{p}_{1/2}, l'j'\rangle_n$ amplitudes.

Using the single-particle widths in the paper by Richard *et al.*[7] and our calculated wave functions, the Γ_p's can be calculated and compared with the experimentally measured ones. This comparison is made in Fig. 4 and one notes that the agreement is quite good. It is seen from Fig. 4 that the calculated levels as a whole shift up about 100 keV compared with the experimental positions.

Some remarks are in order. First, in calculating the proton partial width Γ_p, we have neglected its dependence on the energy of the level under consideration. Secondly, it is pointed out to us by Richard[50] that the partial width Γ_p of the lowest 3^- state was not well measured due to the interfer-

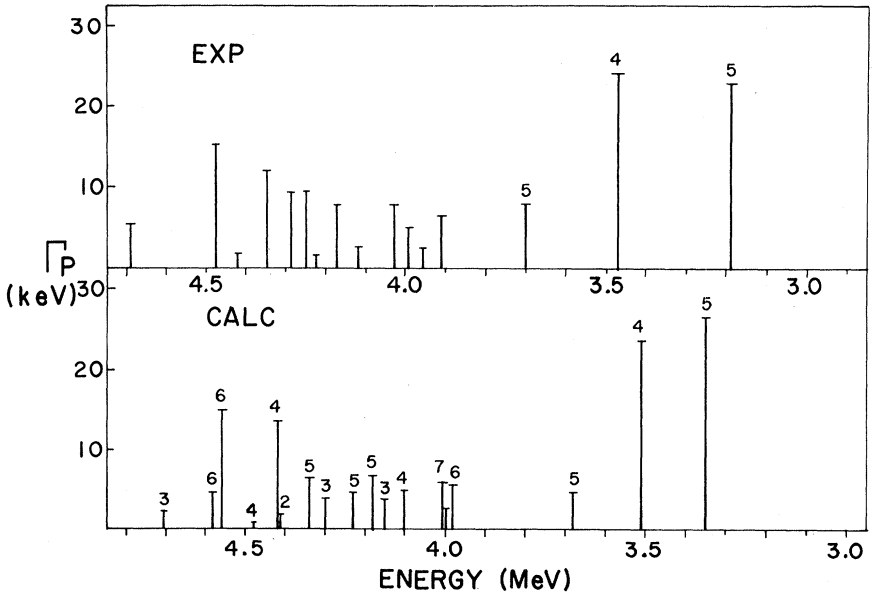

FIG. 4. Proton partial widths for exciting the $\vert\overline{lj}, g_{9/2}\rangle_n$ neutron hole-particle states. The experimental results were taken from Ref. 7. The calculated level energy scale has been arbitrarily shifted upwards by 100 keV.

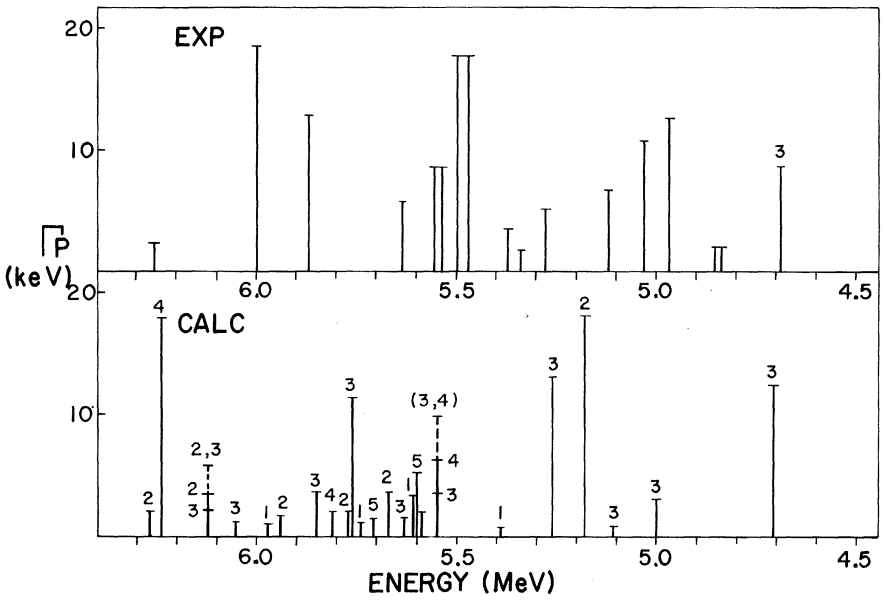

FIG. 5. Proton partial widths for exciting the $|\overline{lj}, d_{5/2}\rangle_n$ neutron hole-particle states. The experimental results were taken from Ref. 8. The double lines indicate doublets.

ence of the direct background, hence it is not included in Fig. 4. Our calculated Γ_p for this lowest 3^- state is $\Gamma_p = 1.63$ keV, a rather small value.

Very recently, Kulleck *et al.*[8] have published their study on the isobaric analog resonance of the Pb^{209} $d_{5/2}$ single-neutron state in Bi^{209}. They have measured the proton partial width Γ_p, which according to Eq. (17), provides a test of the $|\overline{lj}, d_{5/2}\rangle_n$ neutron hole-particle components in our calculated wave functions. This will supplement the information one gathers from the $g_{9/2}$ ground-state analog resonance in Bi^{209} which merely concerns the $|\overline{lj}, g_{9/2}\rangle_n$ hole-particle structure as has already been discussed above.

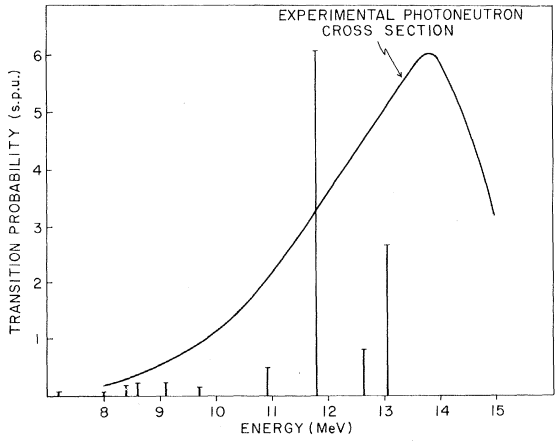

FIG. 6. Distribution of electric dipole strength in Pb^{208}. The experimental results were taken from M. Danos and E. G. Fuller, Ann. Rev. Nucl. Sci. 15, 29 (1965).

Using Eq. (17) and the single-particle widths quoted in the paper by Richard *et al.*,[7] the Γ_p's were calculated and are compared with the experimental results in Fig. 5. The calculated results roughly resemble the measured data, however, the agreement is not as impressive as that for the $|\overline{lj}, g_{9/2}\rangle_n$ hole-particle states. This seems to be expected since the $|\overline{lj}, d_{5/2}\rangle_n$ hole-particle states are all highly excited, for example, their energies generally range from 4.5 to 6.5 MeV. Kulleck *et al.*[8] have assigned the spin of the measured 4.692-MeV level as $J^\pi = 3^-$ which has a measured $\Gamma_p = 8.7$ keV. This seems to be confirmed by our calculation where we find a calculated level at 4.706 MeV with $J = 3^-$ and a calculated $\Gamma_p = 12.4$ keV.

G. Giant Dipole Resonance

Shell-model calculations of the dipole states in Pb^{208} have been performed by Gillet, Green, and Sanderson,[27] and also by Kuo, Blomqvist, and Brown (KBB).[28] We have calculated the $E1$ transition strengths using an effective charge of $0.5e$ (see Sec. V H). The results are plotted in Fig. 6. Our dipole strength is mainly concentrated in the three highest-energy states ranging between 12 to 13 MeV which is about 1 MeV below the experimental peak. The concentration and the location of the peak of the dipole strengths in the present calculation are an improvement over previous calculations which gave less concentration and were centered at lower energies. All the energies

of the dipole states together with their strengths are listed in columns 1 and 2 of Table IX, the wave functions of the lowest nine 1^- states are given in Table X.

It is well known[51-53], for a shell-model calculation of this type where the internal motion and the center-of-mass motion is not separated, that spurious states can be admixed in the calculated eigenstates. The most important spurious state in this case is the state which has the center-of-mass motion in a $1p$ state and with an internal motion the same as the ground state which is known to be in the $1s$ center-of-mass state. In addition to the 28 1^- states given in Table IX, the calculations also produced a 1^- state at -1.62 MeV. This level was not included in Table IX since it is almost completely a spurious state. The amount of spurious-state admixture in any 1^- state can be found by operating on the Pb^{208} ground state with the center-of-mass raising operator[52] and then taking the overlap with the 1^- state in question. For the 1^- state at -1.62 MeV, the overlap integral was calculated to be 0.947.

In contrast, the overlap integrals to the 1^- states at 4.96, 5.39, 5.61, and 5.74 MeV were 0.05, 0.02, 0.06, and 0.10, respectively. Within the accuracy of these calculations, it is concluded that the -1.62-MeV state is essentially a spurious state and that the other states contain very little spurious state admixtures.

KBB[28] mentioned in their paper that the choice of the oscillator parameter $\hbar\omega$ for the single-particle orbitals may have a large effect on the calculated results of the dipole states. In order to investigate this effect, we have, in addition to the present calculation, performed another two additional calculations using the same residual force as described in Sec. III B, but with different values of $\hbar\omega$. One of the calculations used the $(\hbar\omega)_{max}$'s as determined by KLS[38] (see also Sec. III A) for each of the orbitals. The other one used the oscillator parameter adopted in this paper for the proton orbitals, i.e., $\hbar\omega_p = 7.6$ MeV and the oscillator parameter $(\hbar\omega)_{max}$ of the neutron $1j_{15/2}$ orbital for

TABLE IX. The calculated positions of the 1^- levels in Pb^{208} and their respective $E1$ transition rates in Weisskopf spu to the ground state of Pb^{208} when the harmonic-oscillator parameters are fixed by three different prescriptions as explained in the text.

$\hbar\omega_p = \hbar\omega_n = 7.6$ MeV		$(\hbar\omega)_{max}$		$\hbar\omega_p = 7.6$ MeV, $\hbar\omega_n = 9.4$ MeV	
Energy (MeV)	$T(E1)$ (spu)	Energy (MeV)	$T(E1)$ (spu)	Energy (MeV)	$T(E1)$ (spu)
4.96	0.243	4.74	0.071	4.64	0.176
5.39	0.000	5.38	0.093	5.27	0.485
5.61	0.057	5.47	0.841	5.38	0.017
5.74	0.210	5.64	0.469	5.58	0.094
5.97	0.158	5.94	0.213	5.95	0.050
6.06	0.071	6.05	0.042	6.06	0.004
6.37	0.000	6.37	0.000	6.39	0.000
6.67	0.019	6.69	0.022	6.72	0.010
6.81	0.000	6.89	0.007	6.90	0.005
7.14	0.033	7.15	0.054	7.18	0.048
7.22	0.069	7.24	0.028	7.27	0.035
7.26	0.001	7.29	0.101	7.32	0.026
7.46	0.017	7.56	0.015	7.59	0.012
7.58	0.002	7.63	0.068	7.64	0.021
7.68	0.005	7.77	0.041	7.80	0.000
7.85	0.000	7.84	0.084	7.91	0.023
8.02	0.069	8.04	0.063	8.09	0.008
8.19	0.001	8.23	0.000	8.27	0.020
8.42	0.176	8.50	0.020	8.51	0.004
8.65	0.227	8.63	0.892	8.63	0.586
8.95	0.030	8.94	0.015	9.00	0.004
9.11	0.023	9.00	0.021	9.06	0.000
9.16	0.035	9.21	0.455	9.28	0.094
9.71	0.149	9.77	0.157	9.98	0.110
10.90	0.493	11.07	0.080	11.14	0.104
11.81	6.086	12.04	10.11	12.29	4.440
12.64	0.824	12.72	0.659	12.74	0.922
13.05	2.697	12.94	2.267	13.27	6.289

TABLE X. This is a tabulation of the eigenvalues and eigenfunctions of the negative-parity states in Pb^{208}. If more than 10 states of a given spin were calculated, only the lowest 10 states are given. Whenever the calculated amplitude of a given hole-particle configuration is less than 0.1 in magnitude, it is not given. An exception to this rule is that in every case the four largest amplitudes for all states are given even though some may be less than 0.1 in magnitude. The 3^- level at 2.6 MeV is also an exceptional case and its complete wave function is given at the end of the table. The first column gives the spin and parity of the level, and the second column gives the calculated excitation energy. The third column gives the transition rate $T(E\lambda)$ in spu which was calculated by using an effective charge of $0.5e$ as discussed in the text. For each spin, the remaining columns give the hole-particle configurations on top and the corresponding amplitudes below. For example, the amplitude of the $|\bar{h}_{11/2}, i_{13/2}\rangle_p$ configuration for the 1^- level at 4.964 MeV is +0.275. Note that in general, many more configurations were considered than are listed. None of them will appear if their amplitudes are always less than 0.1 for the states given.

I^π	E (MeV)	$T(E\lambda)$ (spu)	Eigenfunctions								
0^-			$\|\bar{p}_{1/2}s_{1/2}\rangle_n$	$\|\bar{f}_{5/2}d_{5/2}\rangle_n$	$\|\bar{h}_{9/2}g_{9/2}\rangle_n$	$\|\bar{p}_{3/2}d_{3/2}\rangle_n$	$\|\bar{d}_{3/2}p_{3/2}\rangle_p$	$\|\bar{s}_{1/2}p_{1/2}\rangle_p$	$\|\bar{f}_{7/2}g_{7/2}\rangle_n$	$\|\bar{g}_{7/2}f_{7/2}\rangle_p$	$\|\bar{d}_{5/2}f_{5/2}\rangle_p$
			$\|\bar{g}_{9/2}h_{9/2}\rangle_p$								
	5.547		−0.863	0.490	−0.074	−0.100					
	6.198		−0.469	−0.817	0.284	−0.170					
	7.332		−0.145	···	0.196	0.919	···	···	−0.288		
	7.693		···	···	0.127	−0.111	0.691	0.673	···	−0.156	−0.122
	7.803		···	0.278	0.904	−0.117	···	−0.203	0.107	0.158	
	8.079		···	···	−0.107	···	0.635	−0.638	···	−0.296	0.283
	9.147		···	···	···	−0.167	···	−0.183	−0.590	−0.235	−0.716
			0.110								
	9.412		···	···	−0.132	−0.116	0.273	···	−0.398	0.854	···
	9.771		···	···	···	0.214	0.185	−0.223	0.619	0.275	−0.573
			0.259								
	13.42		···	···	···	···	···	0.076	−0.095	···	0.237
			0.960								
1^-			$\|\bar{p}_{1/2}s_{1/2}\rangle_n$	$\|\bar{f}_{5/2}d_{5/2}\rangle_n$	$\|\bar{f}_{7/2}g_{9/2}\rangle_n$	$\|\bar{p}_{3/2}d_{5/2}\rangle_n$	$\|\bar{p}_{1/2}d_{3/2}\rangle_n$	$\|\bar{p}_{3/2}s_{1/2}\rangle_n$	$\|\bar{i}_{13/2}j_{15/2}\rangle_n$	$\|\bar{f}_{5/2}g_{7/2}\rangle_n$	$\|\bar{f}_{5/2}d_{3/2}\rangle_n$
			$\|\bar{d}_{5/2}f_{7/2}\rangle_p$	$\|\bar{h}_{9/2}g_{9/2}\rangle_n$	$\|\bar{p}_{3/2}d_{3/2}\rangle_n$	$\|h_{11/2}i_{13/2}\rangle_p$	$\|\bar{f}_{7/2}d_{5/2}\rangle_n$	$\|\bar{s}_{1/2}p_{3/2}\rangle_p$	$\|\bar{d}_{3/2}f_{5/2}\rangle_p$	$\|\bar{h}_{9/2}i_{11/2}\rangle_n$	$\|\bar{d}_{3/2}p_{3/2}\rangle_p$
			$\|\bar{g}_{7/2}h_{9/2}\rangle_p$	$\|\bar{s}_{1/2}p_{1/2}\rangle_p$	$\|\bar{d}_{3/2}p_{1/2}\rangle_p$	$\|\bar{d}_{5/2}p_{3/2}\rangle_p$					
	4.964	0.24	···	···	−0.458	−0.260	−0.205	···	0.349	−0.270	0.166
			−0.374	···	···	0.275	0.157	−0.117	−0.246	0.228	···
			0.168								
	5.392	0.00	−0.857	0.245	0.168	−0.302	···	0.214			
	5.614	0.06	−0.333	0.154	−0.429	0.650	0.427	···	···	−0.156	···
			···	···	···	···	···	0.166			
	5.744	0.21	−0.134	−0.751	···	···	0.194	0.266	−0.155	···	0.248
			···	0.110	···	−0.101	0.287	0.115	···	−0.101	−0.106
			−0.106	···	0.160	0.158					
	5.971	0.16	···	0.258	···	0.352	−0.604	0.191	···	0.216	0.453
			···	···	0.113	···	0.192	···	···	···	···
			···	···	0.139	0.142					
	6.055	0.07	···	0.389	0.236	−0.259	0.440	−0.282	···	−0.194	0.497
			···	−0.117	···	···	0.262	0.101	···	···	···
			···	···	0.127	0.129					
	6.368	0.00	0.264	0.217	···	···	0.204	0.842	···	−0.202	···
			···	···	−0.201	···	−0.188				
	6.670	0.02	···	···	−0.467	−0.173	0.217	···	0.181	0.556	···
			0.226	···	−0.365	···	···	−0.251	0.174	−0.176	
	6.813	0.00	···	···	···	0.140	···	···	···	−0.378	0.152
			0.502	···	0.156	···	···	−0.687	···	0.102	···
			···	−0.166							

TABLE X *(Continued)*

I^π	E (MeV)	$T(E\lambda)$ (spu)	Eigenfunctions								
2^-			$\|\bar{f}_{5/2}g_{9/2}\rangle_n$	$\|\bar{p}_{1/2}d_{5/2}\rangle_n$	$\|\bar{d}_{3/2}f_{7/2}\rangle_p$	$\|\bar{f}_{5/2}d_{5/2}\rangle_n$	$\|\bar{f}_{7/2}g_{9/2}\rangle_n$	$\|\bar{p}_{3/2}d_{5/2}\rangle_n$	$\|\bar{d}_{5/2}h_{9/2}\rangle_p$	$\|\bar{p}_{1/2}d_{3/2}\rangle_n$	$\|\bar{f}_{5/2}s_{1/2}\rangle_n$
			$\|\bar{p}_{3/2}s_{1/2}\rangle_n$	$\|\bar{i}_{13/2}j_{15/2}\rangle_n$	$\|\bar{f}_{5/2}g_{7/2}\rangle_n$	$\|\bar{f}_{5/2}d_{3/2}\rangle_n$	$\|\bar{f}_{7/2}i_{11/2}\rangle_n$	$\|\bar{d}_{5/2}f_{7/2}\rangle_p$	$\|\bar{h}_{9/2}g_{9/2}\rangle_n$	$\|\bar{p}_{3/2}d_{3/2}\rangle_n$	$\|\bar{s}_{1/2}f_{5/2}\rangle_p$
			$\|\bar{h}_{11/2}i_{13/2}\rangle_p$	$\|\bar{s}_{1/2}p_{3/2}\rangle_p$	$\|\bar{d}_{3/2}f_{5/2}\rangle_p$	$\|\bar{h}_{9/2}i_{11/2}\rangle_n$	$\|\bar{g}_{7/2}h_{9/2}\rangle_p$				
	4.422		0.912	−0.353	0.104	···	−0.153				
	5.179		−0.244	−0.836	−0.204	0.194	0.158	0.318			
	5.586		0.166	···	−0.532	−0.223	0.487	−0.388	···	···	···
			···	0.166	0.237	···	···	0.284	···	···	···
			0.205	···	···	0.117					
	5.672		···	−0.103	···	−0.889	−0.167	0.218	···	0.205	0.196
			···	···	···	···	···	···	0.124		
	5.766		···	−0.198	0.714	−0.130	0.508	−0.297	···	···	···
			···	···	···	···	···	···	···	···	···
			···	−0.124							
	5.938		0.117	0.187	0.208	···	···	0.271	···	0.556	−0.306
			−0.121	0.398	···	···	···	0.102	···	0.116	···
			0.318	···	···	0.219	0.216				
	6.009		···	···	···	···	−0.294	0.106	···	−0.543	0.373
			···	0.472	···	···	···	···	···	···	···
			0.328	···	···	0.210	0.214				
	6.120		−0.117	−0.176	···	···	−0.309	−0.457	−0.197	···	−0.474
			0.261	0.237	−0.275	0.247	···	−0.216	···	−0.118	···
			0.140	···	−0.113						
	6.129		···	···	0.104	···	···	···	−0.917	···	0.174
			···	···	···	···	−0.119	···	···	···	0.262
	6.266		···	···	···	−0.197	···	0.379	···	−0.425	−0.567
			−0.134	···	0.316	0.359	···	0.120			
3^-			$\|\bar{f}_{5/2}g_{9/2}\rangle_n$	$\|\bar{p}_{3/2}g_{9/2}\rangle_n$	$\|\bar{d}_{3/2}h_{9/2}\rangle_p$	$\|\bar{f}_{5/2}i_{11/2}\rangle_n$	$\|\bar{p}_{1/2}d_{5/2}\rangle_n$	$\|\bar{s}_{1/2}f_{7/2}\rangle_p$	$\|\bar{d}_{3/2}f_{7/2}\rangle_p$	$\|\bar{f}_{5/2}d_{5/2}\rangle_n$	$\|\bar{f}_{7/2}g_{9/2}\rangle_n$
			$\|\bar{p}_{3/2}d_{5/2}\rangle_n$	$\|\bar{d}_{5/2}h_{9/2}\rangle_p$	$\|\bar{p}_{1/2}g_{7/2}\rangle_n$	$\|\bar{f}_{5/2}s_{1/2}\rangle_n$	$\|\bar{i}_{13/2}j_{15/2}\rangle_n$	$\|\bar{f}_{5/2}g_{7/2}\rangle_n$	$\|\bar{d}_{5/2}f_{7/2}\rangle_p$	$\|\bar{s}_{1/2}f_{5/2}\rangle_p$	$\|\bar{h}_{11/2}i_{13/2}\rangle_p$
			$\|\bar{h}_{9/2}i_{11/2}\rangle_n$	$\|\bar{d}_{3/2}p_{3/2}\rangle_p$	$\|\bar{g}_{7/2}h_{9/2}\rangle_p$						
	4.149	0.01	0.921	0.327	0.141	···	···	···	···	···	−0.069
	4.299	0.02	···	−0.592	0.600	0.365	−0.140	−0.302	···	···	···
			···	···	−0.108	···	···	···	···	−0.108	
	4.706	1.82	0.218	−0.447	−0.395	···	−0.607	0.234	−0.105	···	0.223
			···	···	···	···	0.130	0.104	0.111	···	0.106
	4.996	0.06	···	−0.251	···	0.315	0.299	0.675	0.480	−0.101	···
			···	···	···	···	···	···	−0.129		
	5.106	0.01	···	···	−0.496	0.690	0.163	−0.306	−0.189	···	···
			···	0.202	−0.216						
	5.255	1.25	0.190	−0.299	···	−0.261	0.607	···	−0.262	−0.385	0.290
			···	···	0.125	···	0.198	0.141	···	···	0.111
			0.103								
	5.550	0.25	−0.114	···	···	···	−0.189	−0.257	0.483	−0.670	−0.228
			0.107	···	0.127	0.159	···	···	···	···	0.144
			···	−0.126							
	5.627	0.42	···	···	···	···	0.121	−0.306	0.575	0.499	0.239
			···	···	···	−0.251	0.216	···	0.123	···	0.226
			0.110	···	0.143						
	5.763	0.23	···	···	···	−0.101	0.126	···	···	0.190	−0.477
			0.757	0.258	···	···	0.161				
4^-			$\|\bar{p}_{1/2}g_{9/2}\rangle_n$	$\|\bar{f}_{5/2}g_{9/2}\rangle_n$	$\|\bar{s}_{1/2}h_{9/2}\rangle_p$	$\|\bar{p}_{3/2}g_{9/2}\rangle_n$	$\|\bar{d}_{3/2}h_{9/2}\rangle_p$	$\|\bar{f}_{5/2}i_{11/2}\rangle_n$	$\|\bar{p}_{3/2}i_{11/2}\rangle_n$	$\|\bar{s}_{1/2}f_{7/2}\rangle_p$	$\|\bar{d}_{3/2}f_{7/2}\rangle_p$
			$\|\bar{f}_{5/2}d_{5/2}\rangle_n$	$\|\bar{f}_{7/2}g_{9/2}\rangle_n$	$\|\bar{p}_{3/2}d_{5/2}\rangle_n$	$\|\bar{d}_{5/2}h_{9/2}\rangle_p$	$\|\bar{p}_{1/2}g_{7/2}\rangle_n$	$\|\bar{f}_{7/2}i_{11/2}\rangle_n$	$\|\bar{d}_{5/2}f_{7/2}\rangle_p$		
	3.509		−0.940	0.245	···	0.227	···	···	···	···	···
			···	···	0.048						
	4.066		···	−0.056	−0.873	···	−0.474	···	···	···	···
			···	···	···	0.080					

TABLE X *(Continued)*

I^π	E (MeV)	$T(E\lambda)$ (spu)	Eigenfunctions								
4^-											
	4.104		−0.200	−0.949	···	0.174	···	···	···	···	···
			0.089								
	4.424		−0.238	···	0.118	−0.915	−0.190	···	···	···	···
			···	0.117	0.113						
	4.478		···	···	−0.434	−0.233	0.806	0.282			
	4.859		···	···	0.103	···	−0.266	0.916	0.251		
	5.056		···	···	···	···	···	···	···	0.847	−0.505
			···	0.075	···	···	···	···	−0.079		
	5.341		···	···	···	···	···	···	···	0.483	0.826
			−0.096	···	···	···	···	···	−0.176		
	5.357		···	···	···	···	···	0.212	−0.926	···	···
			···	···	···	···	−0.273	0.102			
	5.551		···	···	···	···	···	···	···	···	0.129
			0.965	0.088	−0.114						
5^-			$\|\bar{p}_{1/2}g_{9/2}\rangle_n$	$\|\bar{f}_{5/2}g_{9/2}\rangle_n$	$\|\bar{p}_{1/2}i_{11/2}\rangle_n$	$\|\bar{s}_{1/2}g_{9/2}\rangle_p$	$\|\bar{p}_{3/2}g_{9/2}\rangle_n$	$\|\bar{d}_{3/2}h_{9/2}\rangle_p$	$\|\bar{f}_{5/2}i_{11/2}\rangle_n$	$\|\bar{p}_{3/2}i_{11/2}\rangle_n$	$\|\bar{d}_{3/2}f_{7/2}\rangle_p$
			$\|\bar{f}_{5/2}d_{5/2}\rangle_n$	$\|\bar{f}_{7/2}g_{9/2}\rangle_n$	$\|\bar{d}_{5/2}h_{9/2}\rangle_p$	$\|\bar{i}_{13/2}j_{15/2}\rangle_n$	$\|\bar{f}_{5/2}g_{7/2}\rangle_n$	$\|\bar{f}_{7/2}i_{11/2}\rangle_n$	$\|\bar{p}_{3/2}g_{7/2}\rangle_n$	$\|\bar{h}_{11/2}i_{13/2}\rangle_p$	
	3.350	10.21	−0.923	···	0.147	0.200	···	0.144	···	···	−0.122
	3.680	14.37	0.289	−0.566	0.357	0.524	0.183	0.186	0.194	···	−0.189
			···	···	···	0.111					
	4.002	0.01	−0.139	−0.698	−0.212	−0.634	···	0.117			
	4.179	1.69	0.130	0.347	0.110	−0.286	0.560	0.647	0.137		
	4.228	0.16	···	···	0.746	−0.283	−0.509	0.209	−0.191	−0.119	
	4.337	0.28	···	···	0.420	−0.136	0.602	−0.561	−0.318	−0.126	
	4.789	1.52	···	0.127	0.146	−0.273	···	−0.370	0.791	···	−0.199
			···	···	0.206						
	5.083	4.25	···	0.130	···	···	···	···	−0.318	0.765	−0.390
			−0.132	0.199	0.136	0.108	0.123				
	5.197	5.17	···	0.149	−0.161	···	···	···	−0.190	−0.593	−0.585
			−0.134	0.331	···	0.146	0.111	0.101	0.107		
	5.596	2.22	···	···	···	···	···	···	···	···	0.322
			−0.830	···	0.328	0.110	···	···	0.103	0.121	
6^-			$\|\bar{f}_{5/2}g_{9/2}\rangle_n$	$\|\bar{p}_{1/2}i_{11/2}\rangle_n$	$\|\bar{p}_{3/2}g_{9/2}\rangle_n$	$\|\bar{d}_{3/2}h_{9/2}\rangle_p$	$\|\bar{f}_{5/2}i_{11/2}\rangle_n$	$\|\bar{p}_{3/2}i_{11/2}\rangle_n$	$\|\bar{f}_{7/2}g_{9/2}\rangle_n$	$\|\bar{d}_{5/2}h_{9/2}\rangle_p$	$\|\bar{i}_{13/2}j_{15/2}\rangle_n$
			$\|\bar{f}_{5/2}g_{7/2}\rangle_n$	$\|\bar{f}_{7/2}i_{11/2}\rangle_n$	$\|\bar{h}_{9/2}g_{9/2}\rangle_n$	$\|\bar{h}_{11/2}i_{13/2}\rangle_p$	$\|\bar{f}_{7/2}d_{5/2}\rangle_n$	$\|\bar{h}_{9/2}i_{11/2}\rangle_n$			
	3.982		0.982	−0.105	−0.142	···	···	···	···	···	···
			···	···	−0.037						
	4.255		−0.107	−0.939	···	···	0.290	−0.136			
	4.562		0.107	···	0.852	0.430	0.211	···	−0.141		
	4.581		···	···	0.464	−0.839	−0.224	···	···	−0.105	
	4.843		···	−0.237	···	0.291	−0.872	−0.283			
	5.120		···	0.200	···	···	0.222	−0.940	···	···	···
			···	0.106							
	5.701		···	···	···	−0.116	···	···	−0.123	0.978	···
			···	0.074							
	5.834		···	···	−0.139	···	···	···	−0.969	−0.126	···
			···	···	···	···	0.106				
	6.483		···	···	···	···	···	···	···	···	0.799
			0.177	0.416	···	0.341	···	0.125			
	6.582		···	···	···	···	···	···	···	···	−0.414
			0.159	0.871	···	−0.147					

TABLE X *(Continued)*

I^π	E (MeV)	$T(E\lambda)$ (spu)	Eigenfunctions								
7^-			$\|\bar{f}_{5/2}g_{9/2}\rangle_n$	$\|\bar{f}_{5/2}i_{11/2}\rangle_n$	$\|\bar{p}_{3/2}i_{11/2}\rangle_n$	$\|\bar{f}_{7/2}g_{9/2}\rangle_n$	$\|\bar{d}_{5/2}h_{9/2}\rangle_p$	$\|\bar{i}_{13/2}j_{15/2}\rangle_n$	$\|\bar{f}_{7/2}i_{11/2}\rangle_n$	$\|\bar{h}_{9/2}g_{9/2}\rangle_n$	$\|\bar{h}_{11/2}i_{13/2}\rangle_p$
			$\|\bar{h}_{9/2}i_{11/2}\rangle_n$	$\|\bar{g}_{7/2}h_{9/2}\rangle_p$	$\|\bar{f}_{7/2}g_{7/2}\rangle_n$	$\|\bar{g}_{7/2}f_{7/2}\rangle_p$					
	4.047	6.47	−0.991	···	0.068	···	···	···	···	···	0.049
			···	···	0.059						
	4.715	3.29	···	0.978	···	···	0.176	0.050	0.049		
	5.092	6.26	0.075	−0.095	0.945	···	0.275				
	5.693	11.90	···	0.163	0.261	−0.456	−0.740	−0.215	−0.261	···	−0.118
			−0.104								
	5.786	0.11	···	···	0.130	0.884	−0.416	···	−0.117		
	6.392	4.97	···	···	···	···	−0.336	0.827	0.105	−0.103	0.377
			···	0.124							
	6.589	0.11	···	···	···	···	−0.224	−0.250	0.924	−0.128	
	6.827	1.10	···	···	···	···	···	−0.143	−0.171	−0.961	···
			···	···	···	−0.103					
	7.021	3.45	···	···	···	···	···	0.397	0.119	−0.148	−0.868
			−0.195								
	7.450	0.43	···	···	···	···	···	−0.089	···	···	−0.236
			0.510	0.818							
8^-			$\|\bar{f}_{5/2}i_{11/2}\rangle_n$	$\|\bar{f}_{7/2}g_{9/2}\rangle_n$	$\|\bar{i}_{13/2}j_{15/2}\rangle_n$	$\|\bar{f}_{7/2}i_{11/2}\rangle_n$	$\|\bar{h}_{9/2}g_{9/2}\rangle_n$	$\|\bar{h}_{11/2}i_{13/2}\rangle_p$	$\|\bar{h}_{9/2}i_{11/2}\rangle_n$	$\|\bar{g}_{7/2}h_{9/2}\rangle_p$	$\|\bar{h}_{9/2}g_{7/2}\rangle_n$
			$\|\bar{g}_{9/2}h_{9/2}\rangle_p$	$\|\bar{g}_{9/2}f_{7/2}\rangle_p$							
	5.026		−0.994	···	···	−0.064	···	···	0.059	···	0.051
	6.103		···	0.984	−0.160	0.060	−0.049				
	6.487		···	0.115	0.880	0.363	···	0.265			
	6.585		···	0.111	0.343	−0.927	···	0.079			
	6.879		···	0.056	0.037	···	0.996	0.046			
	7.038		···	···	0.279	···	···	−0.953	−0.066	−0.063	
	7.663		···	···	···	···	···	−0.107	0.905	0.399	−0.065
	7.957		−0.032	···	···	···	···	···	−0.403	0.913	0.033
	9.679		−0.058	···	···	···	−0.032	···	−0.069	···	−0.995
	11.46		···	···	···	···	···	···	−0.015	−0.033	···
			0.998	0.037							
9^-			$\|\bar{i}_{13/2}j_{15/2}\rangle_n$	$\|\bar{f}_{7/2}i_{11/2}\rangle_n$	$\|\bar{h}_{9/2}g_{9/2}\rangle_n$	$\|\bar{h}_{11/2}i_{13/2}\rangle_p$	$\|\bar{h}_{9/2}i_{11/2}\rangle_n$	$\|\bar{g}_{9/2}h_{9/2}\rangle_p$			
	6.373	17.79	0.862	0.361	−0.134	0.321					
	6.621	4.88	−0.446	0.850	−0.245	0.138					
	6.974	4.95	0.168	0.382	0.697	−0.580					
	7.012	0.40	−0.168	···	0.660	0.725	0.096				
	7.686	0.34	−0.031	···	···	−0.124	0.991	0.043			
	11.55	8.55	−0.031	−0.030	···	···	−0.046	0.998			
3^-			$\|\bar{f}_{5/2}g_{9/2}\rangle_n$	$\|\bar{p}_{3/2}g_{9/2}\rangle_n$	$\|\bar{d}_{3/2}h_{9/2}\rangle_p$	$\|\bar{f}_{5/2}i_{11/2}\rangle_n$	$\|\bar{p}_{1/2}d_{5/2}\rangle_n$	$\|\bar{s}_{1/2}f_{7/2}\rangle_p$	$\|\bar{d}_{3/2}f_{7/2}\rangle_p$	$\|\bar{f}_{5/2}d_{5/2}\rangle_n$	$\|\bar{f}_{7/2}g_{9/2}\rangle_n$
			$\|\bar{p}_{3/2}d_{5/2}\rangle_n$	$\|\bar{d}_{5/2}h_{9/2}\rangle_p$	$\|\bar{p}_{1/2}g_{7/2}\rangle_n$	$\|\bar{f}_{5/2}s_{1/2}\rangle_n$	$\|\bar{i}_{13/2}j_{15/2}\rangle_n$	$\|\bar{f}_{5/2}g_{7/2}\rangle_n$	$\|\bar{f}_{5/2}d_{3/2}\rangle_n$	$\|\bar{f}_{7/2}i_{11/2}\rangle_n$	$\|\bar{d}_{5/2}f_{7/2}\rangle_p$
			$\|\bar{p}_{3/2}g_{7/2}\rangle_n$	$\|\bar{h}_{9/2}g_{9/2}\rangle_n$	$\|\bar{p}_{3/2}d_{3/2}\rangle_n$	$\|\bar{s}_{1/2}f_{5/2}\rangle_p$	$\|\bar{h}_{11/2}i_{13/2}\rangle_p$	$\|\bar{f}_{7/2}d_{5/2}\rangle_n$	$\|\bar{d}_{3/2}f_{5/2}\rangle_p$	$\|\bar{h}_{9/2}i_{11/2}\rangle_n$	$\|\bar{d}_{3/2}p_{3/2}\rangle_p$
			$\|\bar{g}_{7/2}h_{9/2}\rangle_p$	$\|\bar{f}_{7/2}s_{1/2}\rangle_n$	$\|\bar{f}_{7/2}g_{7/2}\rangle_n$	$\|\bar{f}_{7/2}d_{3/2}\rangle_n$	$\|\bar{h}_{9/2}d_{5/2}\rangle_n$	$\|\bar{g}_{7/2}f_{7/2}\rangle_p$	$\|\bar{d}_{5/2}f_{5/2}\rangle_p$	$\|\bar{d}_{5/2}p_{3/2}\rangle_p$	$\|\bar{h}_{9/2}g_{7/2}\rangle_n$
			$\|\bar{h}_{9/2}d_{3/2}\rangle_n$	$\|\bar{d}_{5/2}p_{1/2}\rangle_p$	$\|\bar{g}_{7/2}f_{5/2}\rangle_p$	$\|\bar{g}_{7/2}p_{3/2}\rangle_p$	$\|\bar{g}_{7/2}p_{1/2}\rangle_p$	$\|\bar{g}_{9/2}h_{9/2}\rangle_p$	$\|\bar{g}_{9/2}f_{7/2}\rangle_p$	$\|\bar{g}_{9/2}f_{5/2}\rangle_p$	$\|\bar{g}_{9/2}p_{3/2}\rangle_p$
	2.487	39.37	−0.170	0.372	0.394	0.332	−0.101	0.307	−0.144	−0.046	0.212
			0.075	0.081	0.155	−0.037	0.287	0.141	0.050	0.054	0.167
			0.075	−0.025	0.081	0.137	0.267	0.056	0.105	0.200	−0.084
			0.182	0.033	0.058	0.029	−0.006	−0.031	0.070	0.057	0.039
			0.015	0.060	0.041	−0.014	0.023	0.038	0.038	0.013	0.021

the neutron orbitals, i.e., $\hbar\omega_n = 9.4$ MeV. The results of these two calculations are presented in columns 3 to 6 of Table IX for comparison.

It is interesting to see from Table IX that the calculated energies of the dipole states are similar in all three cases. The transition strengths, on the other hand, are quite sensitive to the types of prescriptions used for $\hbar\omega$. Nevertheless, the position of the giant dipole resonance remains approximately the same in the first two calculations. The third prescription causes the giant dipole resonance to shift upwards to about 13 MeV which is now closer to the experimental value. This upward shift was anticipated by KBB.[28]

H. Electromagnetic Transition Rates

As pointed out in Sec. III, an effective charge concept is necessary because we have used too small a model space in our calculations to be able to describe the observed electromagnetic transitions in Pb^{208}. Although there is no reason to expect the effective charges for different multipolarities to be the same, an effective charge of $0.5e$ for the neutrons and $1.5e$ for the protons gives a fairly good fit to all the observed $E\lambda$ transitions. The $E1$ transitions to the ground state of Pb^{208} have been discussed in Sec. V G. Bernstein[16] has reviewed the status of transition rates in Weisskopf single-particle units for various nuclei which include Pb^{208}. For Pb^{208}, he refers to the experimental results of Alster[14,15] and of Zeigler and Peterson[18] and gives a transition rate of 39.5 ± 2.2 single-particle units (spu) for the decay of the 3^- level at 2.61 MeV to the ground state and two values of 15.8 ± 1.8 and 14 ± 5 spu for the decay of the 5^- level at 3.19 MeV to the ground state. With an effective charge of $0.5e$, we find transition rates of 39.4 spu for the 3^- level and 10.2 spu for the 5^- level which are in good agreement with the experimental results.

VI. CONCLUSIONS

During the past five years or so a large amount of experimental information about the structure of Pb^{208} has become available. Only because of this wealth of experimental data has it been possible to make such a detailed comparison between theory and experiment as has been done here. It is rewarding to see that a conventional shell-model calculation using a simple residual force is able to correlate and explain in a consistent manner much of the detailed structure of the levels in Pb^{206}, Pb^{208}, and Bi^{208}. This is especially gratifying since it was generally believed previously that a TDA calculation would be inadequate for a detailed description of Pb^{208}.

However, one does not expect a calculation of this type to explain all the nuclear structure of Pb^{208} and indeed this is the case here. For example, the positions of the positive-parity states were calculated to be at 3.64 MeV (2^+), 4.95 MeV (4^+), 4.94 MeV (6^+), and 4.81 MeV (8^+) which are to be compared with the experimental results of 4.08 MeV (2^+), 4.32 MeV (4^+), 4.42 MeV (6^+), and 4.60 MeV (8^+), respectively. The high-lying negative-parity states are not as well described as the lower-lying states. The giant dipole resonance and the analog of the Pb^{208} ground state in Bi^{208} are still 1 MeV below the measured data, etc. It is possible that by using an even larger model space and by making a more careful choice of the residual force, the above discrepancies may be removed even within the scope of a conventional shell-model calculation.

The authors would like to thank Professor B. Bayman for remarks concerning the isobaric analog state in Bi^{208}.

---

†Work supported in part by a grant from the U. S. Atomic Energy Commission.

[1]P. Mukherjee and B. L. Cohen, Phys. Rev. 127, 1284 (1962).
[2]C. F. Moore, J. G. Kulleck, P. von Brentano, and F. Rickey, Phys. Rev. 164, 1559 (1967).
[3]S. A. A. Zaidi, J. L. Parish, J. G. Kulleck, C. F. Moore, and P. von Brentano, Phys. Rev. 165, 1312 (1968).
[4]P. Richard, W. G. Weitkamp, W. Wharton, H. Wieman, and P. von Brentano, Phys. Letters 26B, 8 (1967).
[5]J. P. Bondorf, P. von Brentano, and P. Richard, Phys. Letters 27B, 5 (1968).
[6]W. R. Wharton, P. von Brentano, W. K. Dawson, and P. Richard, Phys. Rev. 176, 1424 (1968).
[7]P. Richard, P. von Brentano, H. Weiman, W. Wharton, W. G. Weitkamp, W. W. McDonald, and D. Spalding, Phys. Rev. 183, 1007 (1969).
[8]J. G. Kulleck, P. Richard, D. Burch, C. F. Moore, W. R. Wharton, and P. von Brentano, Phys. Rev. C 2, 1491 (1970).
[9]J. Bardwick and R. Tickle, Phys. Rev. 161, 1217 (1967).
[10]M. Dost and W. R. Hering, Phys. Letters 26B, 443 (1968).
[11]J. H. Bjerregaard, O. Hansen, O. Nathan, and S. Hinds, Nucl. Phys. 89, 337 (1966).
[12]J. H. Bjerregaard, O. Hansen, O. Nathan, R. Chapman, and S. Hinds, Nucl. Phys. A107, 241 (1968).
[13]E. A. McClatchie, C. Glashausser, and D. L. Hendrie, Phys. Rev. C 1, 1828 (1970).
[14]J. Alster, Phys. Rev. 141, 1138 (1966).
[15]J. Alster, Phys. Letters 25B, 459 (1967).
[16]A. M. Bernstein, Phys. Letters 29B, 332, 335 (1969);

in *Advances in Nuclear Physics*, edited by M. Baranger and E. Vogt (Plenum Press, Inc., New York, 1969), Vol. 3, p. 325.
[17]A. R. Barnett and W. R. Phillips, Phys. Rev. 186, 1205 (1969).
[18]J. F. Ziegler and G. A. Peterson, Phys. Rev. 165, 1337 (1968).
[19]J. G. Cramer, P. von Brentano, G. W. Phillips, H. Ejiri, S. M. Ferguson, and W. J. Braithwaite, Phys. Rev. Letters 21, 297 (1968).
[20]E. D. Earle, A. J. Ferguson, G. Van Middelkoop, G. A. Bartholomew, and L. Bergquist, Phys. Letters 32B, 471 (1970).
[21]K. S. R. Sastry, private communication.
[22]N. Stein, C. A. Whitten, Jr., and D. A. Bromley, Phys. Rev. Letters 20, 113 (1968).
[23]J. Sandinos, G. Vallois, O. Beer, M. Gendrot, and P. Lopato, in *Proceedings of the International Conference on Nuclear Physics, Gatlinburg, Tennessee, 12–17 September 1966,* edited by R. L. Becker and A. Zucker (Academic Press Inc., New York, 1967), p. 67.
[24]J. C. Carter, W. T. Pinkston, and W. W. True, Phys. Rev. 120, 504 (1960).
[25]T. T. S. Kuo and W. D. Markiewicz, Bull. Am. Phys. Soc. 12, 538 (1967).
[26]V. Gillet, A. M. Green, and E. A. Sanderson, Phys. Letters 11, 44 (1964).
[27]V. Gillet, A. M. Green, and E. A. Sanderson, Nucl. Phys. 88, 321 (1966).
[28]T. T. S. Kuo, J. Blomqvist, and G. E. Brown, Phys. Letters 31B, 93 (1970).
[29]W. W. True and K. W. Ford, Phys. Rev. 109, 1675 (1958).
[30]W. W. True, Phys. Rev. 168, 1388 (1968).
[31]W. W. True, Phys. Rev. 130, 1530 (1963).
[32]R. Muthukrishnan, private communication.
[33]J. D. Talman and W. W. True, Can. J. Phys. 42, 1081 (1964).
[34]G. Racah, Phys. Rev. 62, 438 (1942); 63, 367 (1943).
[35]P. D. Barnes, E. R. Flynn, G. J. Igo, and D. D. Armstrong, Phys. Rev. C 1, 228 (1970).
[36]I. Talmi, Helv. Phys. Acta 25, 185 (1952).
[37]M. Moshinsky, Nucl. Phys. 13, 104 (1959).
[38]S. Kahana, H. C. Lee, and C. K. Scott, Phys. Rev. 180, 956 (1969).
[39]G. M. Temmer, in *Proceedings of the International Conference on Nuclear Physics, Gatlinburg, Tennessee, 12–17 September 1966,* edited by R. L. Becker and A. Zucker (Academic Press, Inc., New York, 1967), p. 223.
[40]T. T. S. Kuo and G. E. Brown, Nucl. Phys. 85, 40 (1966).
[41]T. T. S. Kuo, Nucl. Phys. A103, 71 (1967).
[42]T. T. S. Kuo, private communication.
[43]In order to be more explicit we now change from our shorthand notation of V_{SE} for the singlet-even force and write it as $V_0 e^{-\beta r^2} P^{SE}$, similarly the triplet-even force is expressed as $V_{TE} = \eta V_0 e^{-\beta r^2} P^{TE}$.
[44]T. T. S. Kuo, Nucl. Phys. A122, 325 (1968).
[45]D. Rowe, Rev. Mod. Phys. 40, 153 (1968).
[46]E. C. Halbert, J. B. McGrory, and B. H. Wildenthal, Phys. Rev. Letters 20, 1112 (1968); E. C. Halbert, J. B. McGrory, B. H. Wildenthal, and S. P. Pandya, in Advances in Nuclear Physics (Plenum Press, Inc., New York, to be published), Vol. 4.
[47]A. Arima, S. Cohen, R. D. Lawson, and M. H. Macfarlane, Nucl. Phys. A108, 94 (1968).
[48]Y. E. Kim and J. O. Rasmussen, Phys. Rev. 135, B44 (1964).
[49]W. T. Pinkston, Nucl. Phys. 53, 643 (1964).
[50]P. Richard, private communication.
[51]J. P. Elliott and T. H. R. Skyrme, Proc. Roy. Soc. (London) A232, 561 (1955).
[52]E. Baranger and C. W. Lee, Nucl. Phys. 22, 157 (1961).
[53]F. Palumbo and D. Prosperi, Nucl. Phys. A115, 296 (1968).